

Reply to comments by Reviewer #1

Thank you very much for useful suggestions which helped us to improve the manuscript.

In the followings, black letters show your comments and blue letters show our reply.

Pages and line numbers are based on the PDF manuscript with track of changes.

General comments:

This manuscript is very good and shows that much of the tropical SS-SR differences (or SSDs) in stratospheric ozone occultation measurements (SAGE II, HALOE, and ACE-FTS) can be explained by the related tidal and seasonal variations of the vertical winds. Among the possible causes of the observed SSDs are (1) systematic instrumental/ retrieval biases for SR and SS ozone, (2) natural diurnal variations, and (3) measurement sampling issues. Although item (1) was not addressed in any detail in this manuscript, items (2) and (3) were considered thoroughly and accounted for mostly with the aid of the SMILES (submillimeter) diurnal ozone dataset and with the model ozone output from SD-WACCM. I recommend that the manuscript be published, but I also urge the authors to correct the important omissions and respond to several of my questions as they relate to the occultation datasets themselves (see below).

Specific comments:

1. Data description: Of primary importance for all three datasets (SAGE II, HALOE, and ACE-FTS) is whether there could be any differences in how they acquire and track the Sun with altitude during SR and SS. As it stands, the reader must accept that all transmission profile measurements were taken, calibrated, and processed to ozone mixing ratios perfectly.

The following description has been added in the revised manuscript (p.5 L22-30):

"Note that there is no systematic difference in the tracking procedure between SR and SS. SAGE II tracks the Sun by moving the field-of-view (FOV) across the solar disk. As the field-of-view went off the edge of the Sun, the scan-mirror reverses direction. HALOE tracks the top edge of the sun, with the science FOV held a fixed angle below this. Extensive SR/SS comparisons have been carried out over the 14-year measurement record and no significant bias in tracking is perceivable. The ACE-FTS is aligned by a tracking system that keeps it pointed at the radiometric center of the sun. While there might exist a very small difference between SR and SS tracking, this has been examined carefully and no significant SR-SS bias exists."

2. SAGE II: SSDs from this experiment are larger than those of the others, particularly in the upper stratosphere (Figure 5), and the authors speculate as to why. With regard to one of your points in Section 5, can you say already whether there are any differences in the diurnal densities between the MERRA and SD-WACCM output?

Figure A1 shows the line plot of diurnal variations in temperature on pressure levels (N.B. on pressure levels, the density changes follow the temperature changes). It is seen that the results from MERRA and SD-WACCM are in good agreement. In this sense, this paragraph seems contradicting to the readers. Thus, in the revised manuscript, we have shortened it and avoided detailed discussion as (p.21 L26—p.22 L2),

“Another related issue may be the reproducibility of tides in SD-WACCM and reanalyses. Satellite measurements use, more or less, (re)analysis data for the altitude registration and/or the retrieval process. It is found that the amplitude of diurnal tide in SD-WACCM and reanalyses is up to ~50% smaller in the upper stratosphere compared to than in data from the Sounding of the Atmosphere using Broadband Emission Radiometry (SABER) measurements (version 2.0 data) (not shown; see Sakazaki et al. 2012 for the comparison between SABER and reanalyses). This could affect any of the satellite datasets, but a further study is needed for a more quantitative discussion.”

3. HALOE: SSDs from HALOE agree well with those from SMILES and SD-WACCM in the upper stratosphere but not so well below about 35 km (Figure 5a) or above 55 km (Figure 8). Therefore, HALOE ozone has anomalies, too. No appropriate reference was given for its Version 19 ozone; refer to Randall et al. (Validation of POAM O3, JGR, 2003) for a more up-to-date and complete discussion. The lack of agreement at 55 km (Figure 8) must be due to photochemical changes at SR and SS rather than to tidal vertical winds and may be correctable in the HALOE algorithm (refer to Natarajan et al., JGR, 2005). Please include a comment about these two anomalies to give a more balanced and fair assessment of the datasets.

Thank you very much for the useful suggestions. Randall et al. (2003) has been added in the revised manuscript (p.7 L15-16).

Because the results from HALOE are consistent with those from other satellite data (Figure 5), we think that the disagreement between the HALOE and SD-WACCM is attributed to any issue in SD-WACCM data. One possible reason is that the diurnal variations in the mesosphere in SD-WACCM

are different from observations (Sakazaki et al., 2013). At the same time, we have mentioned Natarajan et al. (2005) in the manuscript as a possible candidate. The revised manuscript has the following description (p.16 L17-25),

“There is a disagreement in SSD between satellite measurements and SD-WACCM above 55 km (Figure 5). This may be due to the difference in diurnal variations between the model and observations, as shown out by S13 for the altitude region between 50 km and 60 km. S13 also found that such a difference was attributed to the difference in the lowest altitude of the dominance of mesospheric diurnal variations that shows a marked day-night contrast (i.e., ozone concentration maximizes (minimizes) during the nighttime (daytime)). Another possible reason for the disagreement in SSD is that the strong ‘horizontal’ gradient of ozone concentration associated with the rapid ozone changes at SS/SR in the mesosphere was not considered in the retrieval of satellite measurements (Natarajan et al., 2005).”

4. ACE-FTS: Although seasonal sampling is a slight issue in the tropics for these data, I agree that ACE ozone profiles look very good based on the results in Figure 5.

Thank you very much for the friendly comments!

Thank you very much again for your suggestions. Please also refer our reply to Reviewer #2 for further revisions.

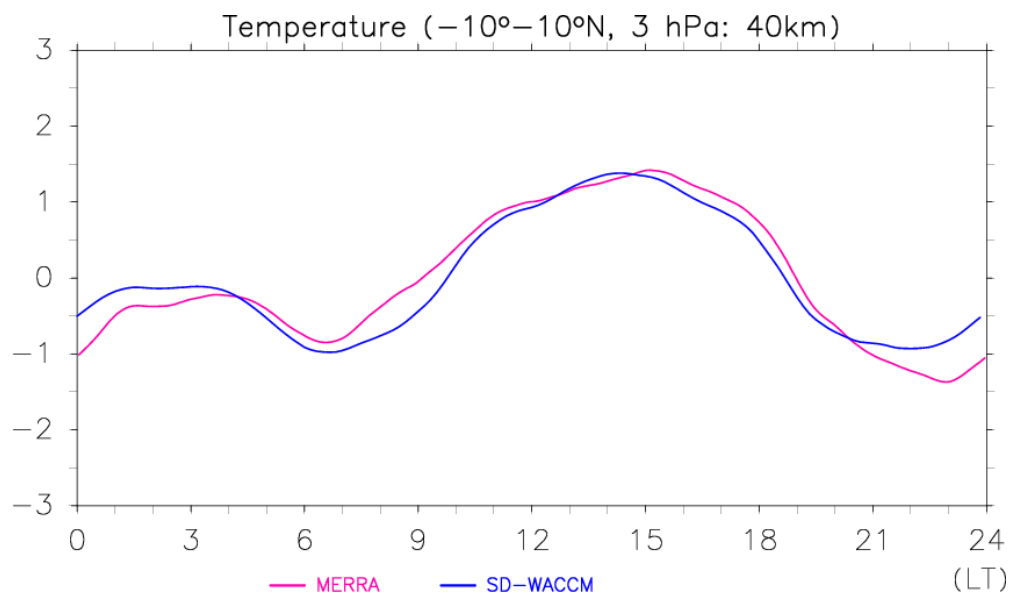


Figure A1: Diurnal temperature variations (K) averaged between 10°S and 10°N at 3 hPa level, as

derived from (purple curve) MERRA and (blue curve) SD-WACCM during 2008-2010.

Reply to comments by Reviewer #2

Thank you very much for useful suggestions which greatly helped us to improve the manuscript.

In the followings, black letters show your comments and blue letters show our reply.

Pages and line numbers are based on the PDF manuscript with track of changes.

This paper represents a careful comparison of various satellite and model estimates of sunrise/sunset differences in (SSD) equatorial ozone. It is well written and considering the number of satellites compared and the inclusion of a model comparison, a remarkably consistent picture emerges of the SSD. My major concern is the attribution of this variation primarily to vertical transport by the migrating diurnal tide.

General comment:

Sakazaki et al. [2012] show the vertical structure of the DW1 (their Figure 5). In the tropics around 40 km the phase of the tide (time of maximum in T) is 1200 – which would imply zero diurnal temperature variation and vertical wind at 0600 and 1800. For a constituent with a vertical gradient and relatively long chemical lifetime we would expect it to roughly be in (or 180 degrees out of) phase with temperature variations (depending on the sign of the constituent vertical gradient – from eqn. 1). Why then do we see a maximum in the transport term when we expect there to be no difference in SR and SS from the DW1? In addition, the authors note that the ozone profile has a relative maximum at 32km (see eqn. 7), which implies the sign of the gradient changes below this level. The vertical wavelength of the tide is about 25 km (again Sakazaki et al. [2012]), so below this relative peak we would expect the same sign in the SR/SS difference - both gradient and wind direction have changed sign, but in Figure 5 we see the sign of SSD has changed. The paper would be far more convincing if it showed both the amplitude and phase of the SD-WACCM DW1 vertical wind (identical to MERRA presumably) and the mean profile of ozone. In addition, the authors have compared these to SABER measurements (16066/12) so it would add to their case if they included those comparisons.

We would appreciate your very careful review and useful suggestions.

Figure B1 shows the vertical profile of amplitude and phase of diurnal migrating tide (DW1) in vertical wind (black curves) and (red curves) averaged at 10°S-10°N, as derived from SD-WACCM data during 2008-2010. As you suggested, the phase basically shows a downward progression but it is almost constant in the middle and upper stratosphere. The constant phase is possibly due to the

trapped mode which maximizes in the upper stratosphere (e.g., Sakazaki et al., 2013). This is why the phase of vertical wind similar between ~20 km and ~40 km; consequently, the sign of SSD is determined by that of vertical gradient of the background ozone profile only.

Next, we consider the phase relationship between the O₃ variations by tidal vertical transport and the temperature variations (Sakazaki et al., 2012). Equation (1) in the text is re-written here:

$$\frac{\partial[\text{O}_3]'}{\partial t} = -w' \frac{\partial[\overline{\text{O}_3}]}{\partial z} + S'. \quad (\text{B1})$$

We assume that you consider the following linearized, thermodynamic equation:

$$\frac{\partial T'}{\partial t} = -w' \left(\frac{d\overline{T}}{dz} + \frac{g}{c_p} \right) + Q, \quad (\text{B2})$$

where T' , w' and Q are DW1 component of temperature (K), vertical wind (m s) and diabatic heating (K s⁻¹), respectively; \overline{T} is zonal-mean, daily-mean temperature; g is gravity constant; c_p is the specific heat at constant pressure.

From Equations (B1-2), we can derive the relationship between T' and $[\text{O}_3]'$. Here it should be noted that the O₃ variations caused by vertical transport are in (or 180 degrees out of) phase with temperature variations only when diabatic heating is negligible ($Q = 0$ in Equation B2). In this case ($Q = 0$), the phases of T' and w' should be apart by a quarter cycle. In SD-WACCM, however, the phases of T' (red curve) and w' (black curve) are almost in phase in the upper stratosphere (Figure B1), indicating that $Q \neq 0$. This will be further discussed in the following paragraph. Note that the phase of T' is ~1200 LT, being consistent with the result by Sakazaki et al. (2012).

Figure B2 shows the diurnal temperature variations at ~40 km from SD-WACCM output. Again, it is seen that the phase is ~1200 LT, as you pointed out. Figure B2 also shows the temperature variations due to adiabatic processes (blue curve; first term on r.h.s. of Eq.B1) and diabatic heating (red curve; second term on r.h.s. of Eq. B1). The sum of the two terms is shown by solid dashed curve; the agreement between solid and dashed curves indicates that the Equation B2 is valid for the present case. It is seen that at this altitude, the two terms with different phases equally contribute to the diurnal variations. Note that the phase of adiabatic processes (i.e., phase of w') is 0600—0900 LT, being out of phase with the O₃ variations caused by vertical transport (Figure 7a in the manuscript); this phase relationship is consistent with your prediction. Note that the phase of ~1200 LT in temperature variations is achieved by the additional variations due to diabatic heating (the

phase is ~1700 LT: red curve in Figure B2).

To summarize, diabatic heating in the upper stratosphere makes the issue complicated; the phases of vertical wind and temperature do not show clear progressions. For the phase relationship between temperature variations and O_3 variations due to vertical transport, it follows your prediction as far as the temperature variation due to adiabatic processes is concerned.

In the revised manuscript, Figure B1 will be added (for vertical wind only). We would not show SABER results for temperature to avoid the complexity.

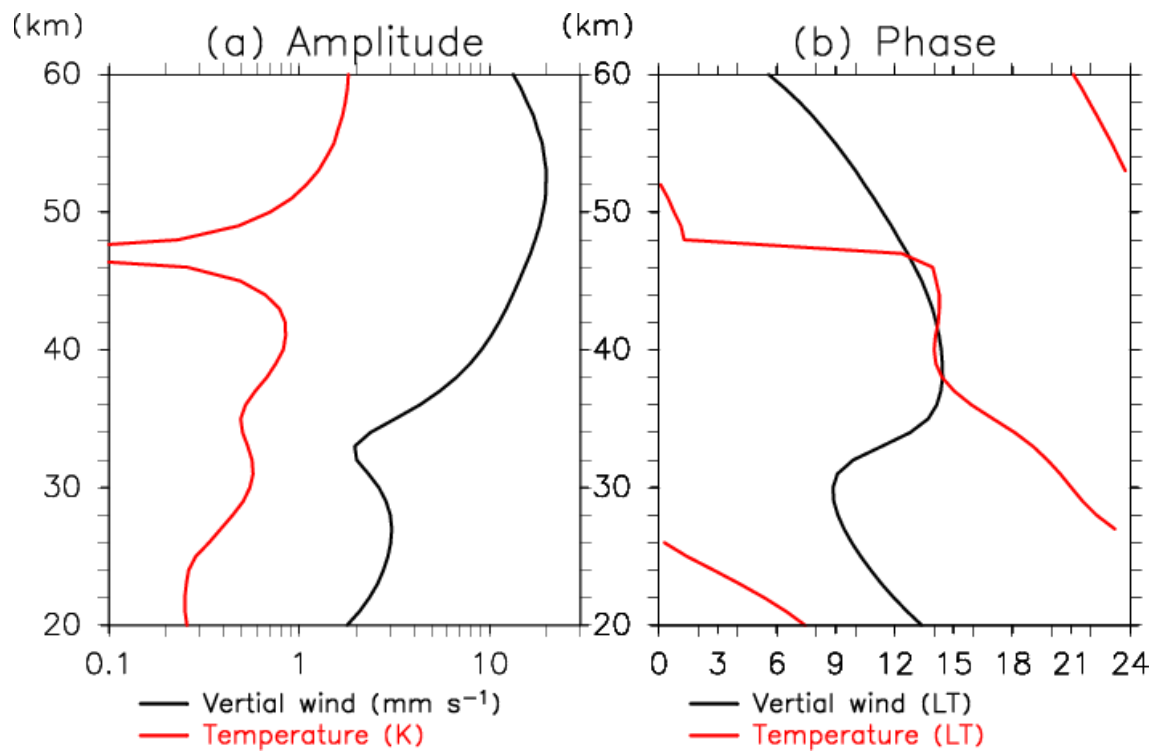


Figure B1: Vertical profiles of (a) amplitude and (b) phase for diurnal migrating tide in (black curves) vertical wind and (red curves) temperature, averaged between 10°S and 10°N, as derived from SD-WACCM data during 2008-2010.

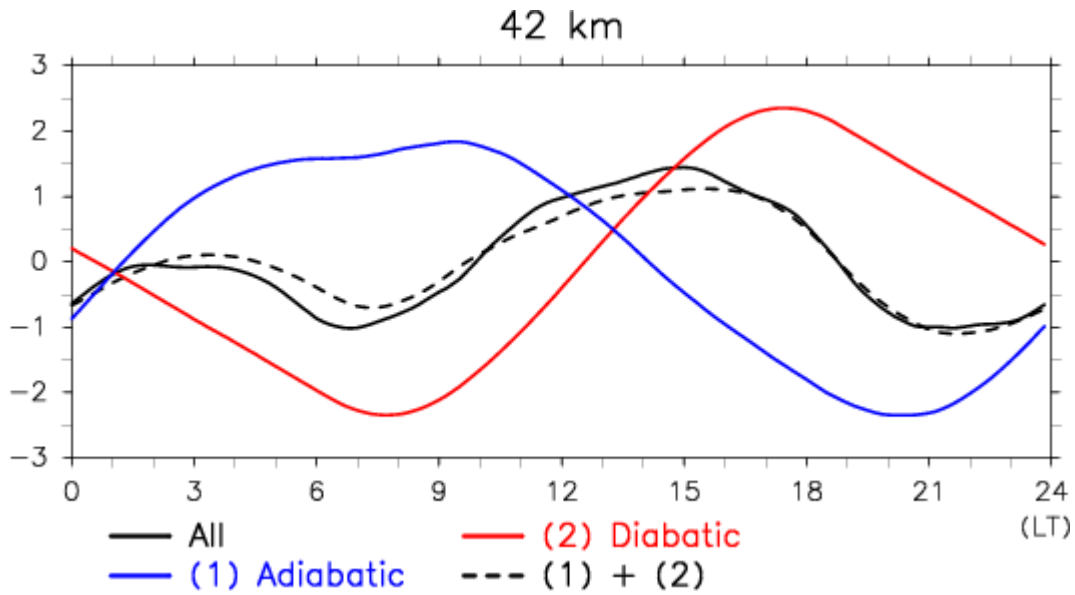


Figure B2: Diurnal temperature variations (K) averaged between 10°S and 10°N at 42 km level, as derived from SD-WACCM data during 2008-2010 (black solid curve). Blue and Red curves denote the contributions from the first and second terms (i.e., temperature variations due to adiabatic processes and diabatic heating), respectively, on the r.h.s. in Equation A2. Black dashed curve shows the sum of the two terms.

Specific comments:

1. 16047/8: "the diurnal migrating tide...is dominant over other higher-order harmonics": This is only true at certain seasons, latitudes and heights. For example, the diurnal tide in temperature and vertical wind is nearly zero at 20 N/S.

Thank you for the suggestion. The expression has been changed as (p.4 L13-14),

"the diurnal migrating tide in upper air... is basically dominant over other higher-order harmonics in the tropical stratosphere."

2. 16047/18: It is true that the vertical wind is small and difficult to measure, but the temperature signal is and has been easily observed and could also be used to infer the vertical wind. It might be worth noting the proposed method is only practical when there is a vertical gradient in the constituent.

Thank you for the suggestion. The expression has been revised as (p.4 L23-24),

“We suggest that in the presence of vertical gradient of ozone, the ozone SSD could be used to obtain quasi-observational evidence of tidal vertical winds in the tropical stratosphere.”

The temperature tide may be difficult to use for estimating the vertical wind in the presence of diabatic heating ($Q \neq 0$). Please see our reply to the general comment.

3. 16053/25: Can the authors estimate an uncertainty in the geometric altitude determination?

The following description has been added in the revised manuscript (p.10 L12-15):

“The uncertainty in altitude registration for SMILES is considered to be in the same order as that for other datasets. Note that there is no systematic difference in the altitude registration between SR and SS.”

4. 16054/10: what is the frequency of the MERRA data used to nudge SD-WACCM? Enough to resolve the diurnal tides?

6-hourly data are used in this study. In the revised manuscript, the corresponding sentence has been revised as (p.10 L24-27),

“Here specified dynamics (SD)-WACCM is a chemical transport model (CTM) that nudges WACCM4 temperature, horizontal winds, and surface pressure towards 6-hourly time series from MERRA reanalysis (Rienecker et al., 2011) below 50 km.”

Please also see Figure A1 (on the reply to Reviewer #1) which compares the diurnal temperature variations at 42 in SD-WACCM and MERRA. The two results are in good agreement.

5. 16060/24: Without error bars on these differences, it is difficult to say how similar these results are. Can the authors estimate the uncertainties in SSD based on simple propagation of errors?

We have added error bars (95% confidence interval) to the SAGE II, HALOE and ACE-FTS results in Figure 5. Please see Figure B3 for the revised version. The procedure to obtain the confidence interval is as follows. First, the ‘error’ is defined as the standard deviation from the monthly composite value. Then the error for the annual-mean has been derived such that the

errors for each month propagate into the annual mean. Finally, the statistical test (t -test) has been made with the degrees of freedom being the total number of SS-SR pairs (128 for SAGE II, 86 for HALOE and 25 for ACE-FTS).

Accordingly, we have added error bars for Figure 10 (seasonal variation of SSD; Figure 9 in the original manuscript). Please see Figure B4 below for the revised version.

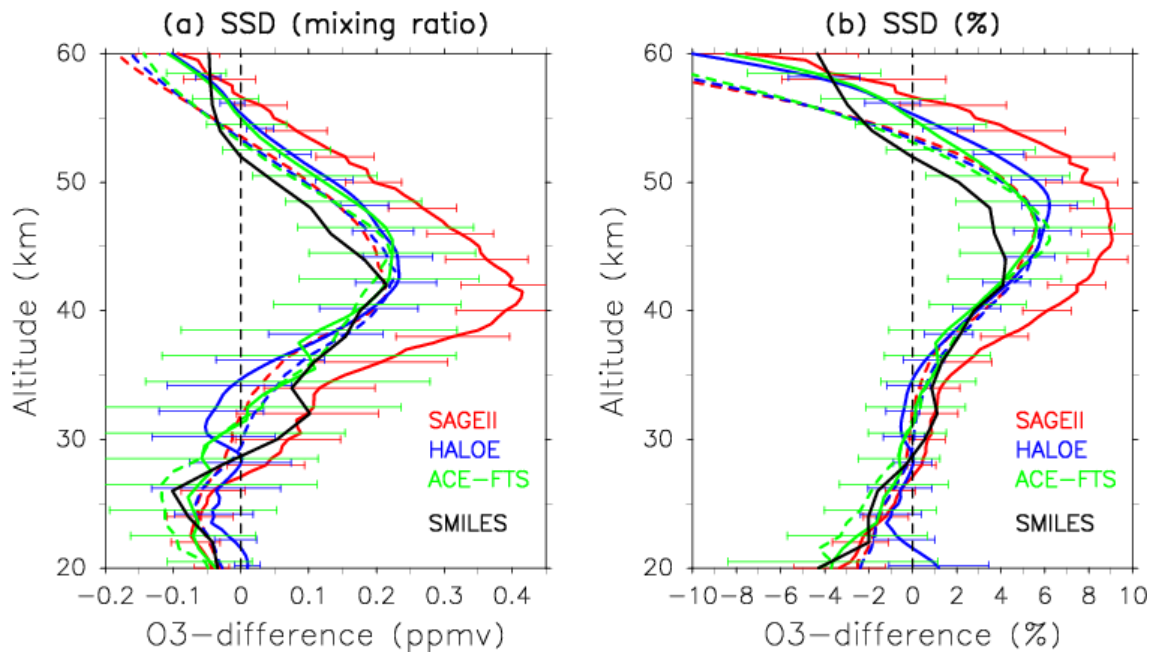


Figure B3: Revised Figure 5. SSD for 10°S–10°N in (a) ozone mixing ratio (ppmv), 2 and (b) SSD ratio to the daily mean (%), derived from SAGE II (red solid curves), HALOE (blue solid curves), and ACE-FTS (green solid curves). Red, blue, and green dashed curves denote SD-WACCM results at SAGE II, HALOE, and ACE-FTS coincidence, respectively. Black solid curves show the SMILES result (SR and SS are defined by those profiles with a solar zenith angle between 80° and 100°). Black dot-dashed curves show the difference between 18:00 and 06:00 LT, calculating using SMILES data and based on 1 hourly diurnal variations. Horizontal bars for SAGE II, HALOE and ACE-FTS show 95% confidential levels in t -test. For the statistical test, the error is defined as the standard deviation for the monthly SSD; this quantity has been propagated to the error in annual-mean. Then, the t -test has been made with the degrees of freedom being the total numbers of SS-SR pairs for each dataset.

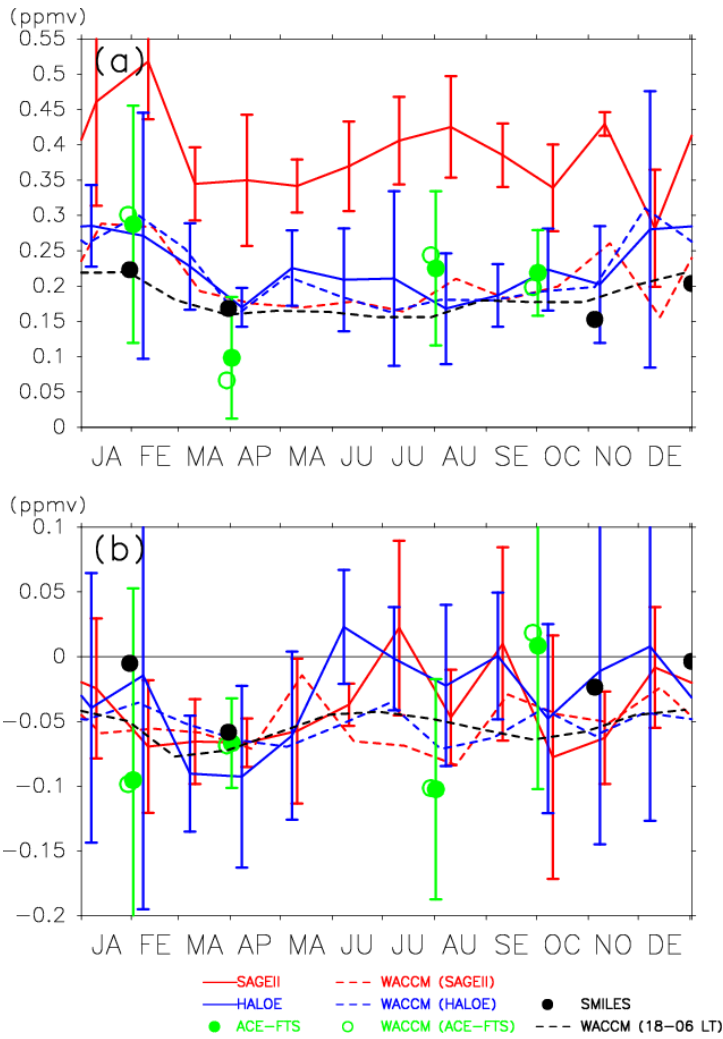


Figure B4: Revised Figure 10. Seasonal variation of O₃ SSD at altitudes of (a) 40–45 km and (b) 22–28 km, obtained from (red solid curve) SAGE II, (red dashed curve) SD–WACCM at SAGE II locations, (blue solid curve) HALOE, (blue dashed curve) SD–WACCM at HALOE locations, (green closed circles) ACE–FTS, (green open circles) SD–WACCM at ACE–FTS locations, and (black closed circles) SMILES. The black dashed curve shows the difference in ozone between 18:00 and 06:00 LT, as deduced from diurnal variations in ozone concentration based on full-grid SD–WACCM between 2008. Vertical bars for SAGE II, HALOE and ACE–FTS show 95% confidential levels with *t*-test.

- 16062/27: Again, "quasi-observation evidence of seasonal variations in stratospheric vertical tidal winds" can be obtained directly from temperature observations – simply replace dO_3/dz with dT/dz .

The term of “for the first time” has been removed from the text to soften the expression (p.18 L15).

7. 16065/13: see general comment - how can the sign change when the gradient in ozone changes sign but the 15 km difference in altitude is less than the vertical wavelength of the DW1 tide?

The phase of vertical wind does not show a downward progression in the upper stratosphere possibly due to the trapped mode. This is why the sign of SSD is only determined by that of vertical gradient of background of O₃.

Please see the discussion above on your general comment and Figure B1 for details.

The following description has been added (p.17 L28—p.18 L3):

“Figure 8 shows the amplitude and phase of diurnal migrating tide in vertical wind averaged between 10°S and 10°N, as derived from SD-WACCM data. The amplitude exponentially increases with altitude. The phase basically shows the downward progression but it is almost constant around 40 km possibly due to the presence of trapped modes excited by ozone heating (e.g., Sakazaki et al., 2013b). Consequently, the phase of vertical wind is similar in the whole stratosphere; thus, the sign of SSD (i.e., negative at 20-30 km and positive at 35-50 km) is determined by that of vertical gradient in the background ozone concentration.”

8. 16066/12: How do the authors explain the good agreement in SSD between SDWACCM and observations, when the tidal amplitudes in SD-WACCM/MERRA are a factor of two low?

We had this description because it might be possible that observations which depend on reanalyses and SD-WACCM in the altitude registration and/or retrieval process show small SSD. But this paragraph seems confusing to the readers so that we shortened it and avoided detailed discussion (p.21 L26—p.22 L2).

“Another related issue may be the reproducibility of tides in SD-WACCM and reanalyses. Satellite measurements use, more or less, (re)analysis data for the altitude registration and/or the retrieval process. It is found that the amplitude of diurnal tide in SD-WACCM and reanalyses is up to ~50% smaller in the upper stratosphere compared to than in data from the Sounding of the Atmosphere using Broadband Emission Radiometry (SABER) measurements (version 2.0 data) (not shown; see Sakazaki et al. 2012 for the comparison between SABER and reanalyses). This could affect any of the satellite datasets, but a further study is needed for a

more quantitative discussion.”

9. 16077/Figure 5: If this is SSDcorr the caption should reflect that.

Corrected. Thank you.

10. 16083/Figure 11: This only shows the amplitude, but to understand the transport, the phase of the migrating tide needs also to be shown.

The vertical profile of amplitude and phase of diurnal migrating tide in vertical wind (black curves in Figure B1), has been added in the revised manuscript with the following description (p17 L28—p.18 L3) :

“Figure 8 shows the amplitude and phase of diurnal migrating in vertical wind averaged between 10°S and 10°N, as derived from SD-WACCM data. The amplitude exponentially increases with altitude. The phase basically shows the downward progression but it is almost constant around 40 km possibly due to the presence of trapped modes excited by ozone heating (e.g., Sakazaki et al., 2013b). Consequently, the phase of vertical wind is similar in the whole stratosphere; thus, the sign of SSD (minus at 20-30 km and plus at 35-50 km) is determined by that of vertical gradient in the background ozone concentration.”

Thank you very much again for your suggestions. Please also refer our reply to Reviewer #1 for further revisions.

Reference

Sakazaki, T., M. Fujiwara, and X. Zhang (2013), Interpretation of the vertical structure and seasonal variation of the diurnal migrating tide from the troposphere to the lower mesosphere. *Journal of Atmospheric and Solar-Terrestrial Physics*, 105-106, 66-80, doi:10.1016/j.jastp.2013.07.010.

1 **Sunset–Sunrise Difference in Solar Occultation Ozone**
2 **Measurements (SAGE II, HALOE, and ACE–FTS) and its**
3 **Relationship to Tidal Vertical Winds**

4
5 **T. Sakazaki¹, M. Shiotani¹, M. Suzuki², D. Kinnison³, J. M. Zawodny⁴, M. McHugh⁵,**
6 **and K. A. Walker⁶,**

7
8 [1]{Research Institute for Sustainable Humanosphere, Kyoto University, Uji, Japan}

9 [2]{Institute of Space and Astronautical Science, Japan Aerospace Exploration Agency,
10 Sagamihara, Japan}

11 [3]{National Center for Atmospheric Research, Boulder, USA}

12 [4]{NASA Langley Research Center, Hampton, USA}

13 [5]{Global Atmospheric Technologies and Sciences, Newport News, USA}

14 [6]{Department of Physics, University of Toronto, Toronto, Canada}

15
16 Correspondence to: T. Sakazaki (takatoshi_sakazaki@rish.kyoto-u.ac.jp)

17
18 **Abstract**

19 This paper contains a comprehensive investigation of the sunset–sunrise difference (SSD; i.e.,
20 the sunset-minus-sunrise value) of the ozone mixing ratio in the latitude range of 10°S–10°N.
21 SSD values were determined from solar occultation measurements based on data obtained
22 from the Stratospheric Aerosol and Gas Experiment (SAGE) II, the Halogen Occultation
23 Experiment (HALOE), and the Atmospheric Chemistry Experiment Fourier Transform
24 Spectrometer (ACE-FTS). The SSD was negative at altitudes of 20–30 km (–0.1 ppmv at 25
25 km) and positive at 30–50 km (+0.2 ppmv at 40–45 km) for HALOE and ACE–FTS data.
26 SAGE II data also showed a qualitatively similar result, although the SSD in the upper
27 stratosphere was two times larger than those derived from the other datasets. On the basis of

1 an analysis of data from the Superconducting Submillimeter Limb Emission Sounder
2 (SMILES), and a nudged chemical-transport model (the Specified Dynamics version of the
3 Whole Atmosphere Community Climate Model: SD-WACCM), we conclude that the SSD
4 can be explained by diurnal variations in the ozone concentration, particularly those caused by
5 vertical transport by the atmospheric tidal winds. All datasets showed significant seasonal
6 variations in the SSD; the SSD in the upper stratosphere is greatest from December through
7 February, while that in the lower stratosphere reaches a maximum twice: during the periods
8 March–April and September–October. Based on an analysis of SD-WACCM results, we
9 found that these seasonal variations follow those associated with the tidal vertical winds.

10

11 **1 Introduction**

12 Stratospheric ozone (O_3) plays a critical role in the climate system through radiative processes,
13 while simultaneously protecting the Earth's surface from harmful ultraviolet radiation. Since
14 the discovery of the ozone hole, long-term changes in ozone concentration have been studied
15 extensively using various ground-based and satellite measurements (WMO, 2011). Useful
16 datasets for long-term monitoring of vertical profiles of ozone levels can be obtained from
17 solar occultation instruments, such as the Stratospheric Aerosol and Gas Experiment (SAGE)
18 II (McCormick, 1987; McCormick et al., 1989), the Halogen Occultation Experiment
19 (HALOE) (Russell et al., 1993), and the Atmospheric Chemistry Experiment Fourier
20 Transform Spectrometer (ACE-FTS) (Bernath et al., 2005), as they have measurements that
21 are self-calibrating and have high sensitivity. These measurements have been used to detect
22 seasonal and interannual variability, as well as long-term trends, in the stratospheric ozone
23 concentration (e.g., Shiotani and Hasebe, 1994; Randell and Wu, 1996; Newchurch et al.,
24 2003; WMO 2011; Kyrölä et al., 2013).

25 These solar occultation instruments measure the atmosphere at sunrise and sunset (hereafter
26 SR, SS). It has been reported that there is a difference in the observed values between the SR
27 and SS profiles (hereafter, this is referred to as the sunset–minus-sunrise difference, SSD).
28 For SAGE II, the SSD is reported to be up to 10% between altitudes of 35 and 55 km, with a
29 maximum occurring in the tropics (cf. SAGE II version 5.9 data: Wang et al., 1996; version
30 6.2 data: McLinden et al., 2009; version 7.0 data: Kyrölä et al., 2013). For HALOE (version
31 17 data), Brühl et al. (1996) reported an SSD of approximately 5% in the tropical stratopause.

1 SSD values based on ACE–FTS (Fourier Transform Spectrometer) observations have yet to
2 be reported, as far as we know.

3 Quantification of the SSD and a understanding the source of this difference are necessary for
4 the construction of combined datasets from SR and SS profiles. As we will explore in this
5 study, the SSD could be caused by any one of three factors, including: (1) systematic
6 instrumental/retrieval bias between SR and SS observations; (2) natural diurnal variations;
7 and (3) sampling issues. The factor (3) relates to the fact that if the times of SR and SS
8 measurements are considerably different, the background ozone concentration changes
9 (background changes occur on timescales longer than a day; e.g., subseasonal variations)
10 during such periods are misinterpreted as an example of SSD (see Section 3 for details). In
11 this sense, such spurious contributions, or contamination, should be assessed and removed
12 before discussing the SSD.

13 In previous studies, the ozone SSD was mainly attributed to factor (1); in other words, factor
14 (2) was thought to be negligible (Wang et al., 1996; Brühl et al., 1996). This was because
15 diurnal variations in stratospheric ozone level were considered to be small and/or to be
16 symmetric between SS and SR, if only photochemistry processes are taken into account.
17 However, note that there are few observations of diurnal variations in the stratosphere and,
18 thus, the above assumption had not been confirmed. In addition, factor (3) may not have been
19 properly considered in some studies (e.g., in the context of interannual variations of the SSD,
20 as shown by Kyrölä et al. 2013; see Section 3).

21 Recently, Sakazaki et al. (2013a; hereafter S13) revealed diurnal variations in ozone
22 concentration from the lower to upper stratosphere using data from both the Superconducting
23 Submillimeter Limb Emission Sounder (SMILES) and chemical-transport models (CTMs).
24 They showed that the peak-to-peak difference in ozone levels reaches 8% during a day. An
25 important point here is that, at some altitudes, the diurnal variations exhibit asymmetric ozone
26 levels when comparing measurements at SS and SR, with the SSD reaching around 4% in the
27 upper stratosphere. S13 showed that the diurnal variations ($[O_3]'$) are largely controlled by the
28 following equation,

29
$$\frac{\partial [O_3]'}{\partial t} = -w' \frac{\partial [\overline{O_3}]}{\partial z} + S' \quad (1),$$

30 where t represents time, w' the diurnal variations in the vertical winds (tidal vertical winds), z
31 altitude, $[\overline{O_3}]$ the daily, zonal mean ozone, and S' the diurnal variations in chemical

1 production or loss. The first term on the right-hand-side denotes the dynamical variation due
2 to vertical transport by atmospheric tidal winds, while the second term denotes the
3 photochemical variation. It should be noted that the dynamical variation results in a maximum
4 at 1800–2000 local time (LT) in the upper stratosphere (and at 0000–0600 LT in the lower
5 stratosphere; cf. figure 7d of S13), possibly causing a positive (negative) SSD. In contrast,
6 although the photochemical variations are also important above an altitude of 30 km during
7 the daytime, they are almost zero at SR/SS (see figure 7b of S13), and so do not contribute to
8 the SSD. This has already been demonstrated and discussed in previous studies (e.g., Pallister
9 and Tuck, 1984; Wang et al., 1996; Brühl et al., 1996). For the tropical mesosphere and lower
10 thermosphere, Marsh and Russell (2000) used HALOE data to attribute the SSD of nitric
11 oxide (NO) to diurnal variations caused by tidal vertical transport.

12 With regard to tides, the diurnal migrating tide (i.e., the diurnal harmonic component, which
13 does not depend on longitude, but only on the LT of a particular latitude band) is basically
14 dominant over other higher-order harmonics in the tropical stratosphere. Vertical winds
15 associated with the diurnal migrating tide become maximal in the tropics, so that diurnal
16 variations in ozone levels caused by vertical transport also reach a maximum in the tropics
17 (see figure 8 of S13). In the tropical stratosphere, the diurnal migrating tide is known to
18 exhibit a significant seasonal dependence, with its amplitude reaching a peak in January–
19 February and July–September, as seen in satellite-based temperature measurements (e.g., Wu
20 et al., 1998; Zeng et al., 2008; Huang et al., 2010; Sakazaki et al., 2012). These findings
21 suggest that the tidal vertical winds and, consequently, the SSD, also show similar seasonal
22 variations. Note that the tidal vertical wind is relatively difficult to observe directly because of
23 its rather small amplitude. We suggest that in the presence of vertical gradient of ozone, the
24 SSD pertaining to the ozone levels could be used to obtain quasi-observational evidence of
25 tidal vertical winds in the tropical stratosphere.

26 As outlined above, SSDs have been noticed but they were considered independently for each
27 occultation instrument. In addition, they have not been investigated fully in terms of diurnal
28 ozone variations. The purpose of this study is, first, to quantify the SSD, including its
29 seasonal dependence, by analyzing and comparing data from three independent solar
30 occultation instruments: SAGE II, HALOE, and ACE-FTS. The differences among the
31 datasets due to differences in measurement times are discussed with the aid of CTM data
32 (from the Specified Dynamics version of the Whole Atmosphere Community Climate Model:

1 SD–WACCM), which provides a homogeneous dataset covering the full operational periods
2 of each of the three satellite missions. Next, we interpret the SSD in terms of diurnal
3 variations based on SMILES measurements and three-hourly, 3D-gridded SD–WACCM data,
4 which provide data not only at SR/SS, but for the full diurnal cycle. The 3D-gridded SD–
5 WACCM data are also used to discuss diurnal variations related to vertical transport and
6 photochemistry. This study focuses on the tropical stratosphere at latitudes of 10°S–10°N
7 between 20 and 60 km in altitude, as the SSD is greatest in the tropics. The remainder of this
8 article is organized as follows. Sections 2 and 3 describe the datasets and analysis methods,
9 respectively. Section 4 describes the SSD and its seasonal variations, and we also discuss the
10 contribution from diurnal ozone variations. Section 5 summarizes our main results.

11

12 **2 Data Description**

13 In this study, the average SSD in the tropical stratosphere within the latitude range 10°S–
14 10°N is analyzed and discussed using data from the three solar occultation instruments:
15 SAGE II, HALOE, and ACE–FTS. To quantify the SSD caused by natural diurnal variations
16 in ozone concentration, data from SMILES limb emission measurements are also analyzed. In
17 addition, two datasets from SD–WACCM are used: the satellite coincidence data subset and
18 the full three-hourly, 3D-gridded data. The former is used to discuss the difference in SSD
19 among the different satellite datasets, while the latter is used to consider the SSD in terms of
20 diurnal variations. All data are analyzed at geometric altitudes in the stratosphere between 20
21 and 60 km.

22 Note that there is no systematic difference in the tracking procedure between SR and SS.
23 SAGE II tracks the Sun by moving the field-of-view (FOV) across the solar disk. As the field-
24 of-view went off the edge of the Sun, the scan-mirror reverses direction. HALOE tracks the
25 top edge of the sun, with the science FOV held a fixed angle below this. Extensive SR/SS
26 comparisons have been carried out over the 14-year measurement record and no significant
27 bias in tracking is perceivable. The ACE-FTS is aligned by a tracking system that keeps it
28 pointed at the radiometric center of the sun. While there might exist a very small difference
29 between SR and SS tracking, this has been examined carefully and no significant SR-SS bias
30 exists. Further details are provided in the following subsections.

1 2.1 SAGE II

2 The SAGE mission has deployed three instruments; i.e., SAGE I, II, and III. This study
3 uses data from SAGE II because these measurements cover the longest period. SAGE II was
4 launched in October 1984 on board the Earth Radiation Budget Satellite (ERBS) and
5 remained operational until August 2005, providing data for over 21 years. The ERBS
6 operated in a 610 km altitude, circular orbit with an inclination of 56°. SAGE II is a seven-
7 channel spectrometer capable of obtaining ozone levels from measurements in the 600 nm
8 Chappius band (McCormick et al., 1987, 1989).

9 Figure 1a shows the SAGE II measurement locations obtained in 1992. The latitude coverage
10 ranges from 80°S to 80°N. SAGE II performed two occultation measurements per orbit,
11 sampling two narrow latitude regions each day. As a result, for each day up to 15 SR and 15
12 SS profiles were obtained near the same latitude regions, but spaced some 24° apart in
13 longitude. Approximately 10 times per year, the tracks of the SR and SS measurements
14 crossed over. The sampling pattern (i.e., the measurement day of the year at a particular
15 latitude) changed gradually from year to year, and so cover the whole year when data are
16 collected for several years.

17 We analyzed SAGE II version 7.0 data (Damaedo et al., 2013) obtained during the period
18 1985–2005. Data were provided for geometric altitudes between 0 and 70 km at intervals of
19 0.5 km. Geometric altitudes were determined by the viewing geometry with the aid of data
20 from the Modern Era-Retrospective Analysis for Research Applications (MERRA) reanalysis
21 (Rienecker et al., 2011). The uncertainty in altitude registration is less than 20 m (Damaedo et
22 al., 2013). Ozone mixing ratio is calculated as the ratio of ozone number density to
23 atmospheric density, both of which are provided in SAGE II data. The atmospheric density is
24 not measured by SAGE II but derived from MERRA data; however, the results of SSD (%)
25 (cf. Figure 5b) do not change even if the following analysis is done based on ozone number
26 density. Prior to our detailed analysis, data were screened following the guidelines provided
27 in the SAGE II version 7.0 readme file
28 (https://eosweb.larc.nasa.gov/project/sage2/sage2_release_v7_notes), as follows. Any profile
29 with an error estimate larger than 10% at altitudes between 30 and 50 km was rejected. Data
30 points with an uncertainty estimate of 300% or greater were rejected. Data points at the
31 altitude of and below the occurrence of an aerosol extinction value greater than 0.006 km⁻¹
32 were rejected. Data points at the altitude of and below the occurrence of both the 525 nm

1 aerosol extinction value exceeding 0.001 km^{-1} and the 525/1020 extinction ratio of less than
2 1.4 were rejected. Data points pertaining to altitudes below 35 km with an uncertainty
3 estimate of 200% (or larger) were rejected. On the basis of this screening process, 3.9% and
4 5.6% of all profiles were rejected for the times of SR and SS, respectively.

5 **2.2 HALOE**

6 HALOE was launched in September 1991 on board the Upper Atmosphere Research Satellite
7 (UARS) and remained operational until November 2005, providing data over 15 years. UARS
8 was placed in a 585 km circular orbit, with an inclination of 57° (Russell et al., 1993). Its
9 ozone measurements were made at mid-infrared (mid-IR) wavelengths ($9.6 \mu\text{m}$).

10 The HALOE measurement locations during 1992 are shown in Figure 1b. The latitude
11 coverage was approximately 80°S – 80°N . The instruments measured up to 15 SR and 15 SS
12 profiles each day. Approximately 10 times per year, the tracks of the SR and SS
13 measurements crossed over. As with SAGE II, the sampling pattern of HALOE changed
14 gradually from year to year.

15 We analyzed HALOE version 19 data obtained over the period 1991–2005 ([e.g., Randall et al.,](#)
16 [2003](#)). Data were provided at 271 pressure levels; i.e., $1000 \times 10^{-(i-1)/30}$ hPa ($i = 1, 2, \dots, 271$),
17 between 1000 and 10^{-6} hPa, with a corresponding vertical spacing of approximately 0.5 km.
18 Geometric altitudes were also provided in relation to the pressure levels for each profile, so
19 that we mapped ozone mixing-ratio data onto geometric altitude levels between 0 and 70 km,
20 with a spacing of 0.5 km. No screening was performed on the HALOE data.

21 HALOE profiles are registered in altitude in an iterative fashion, and the resulting registration
22 is generally assessed to be better than 100 m (McHugh et al., 2003, 2005). Initially, the data
23 are placed on an altitude grid based on the HALOE measurements versus zenith angle. A first
24 pressure registration is performed using the measured transmittance profile from the $2.8 \mu\text{m}$
25 channel (dominated by CO_2 absorption). In this process, the altitude grid is shifted to best
26 match simulated transmittances in the 30 to 45 km altitude range, assuming the temperature
27 profile from the National Center for Environmental Prediction (NCEP) reanalysis (Beaver et
28 al., 1994; Remsberg et al., 2002; see Kalnay et al., 1996 for NCEP reanalysis). Temperatures
29 and corresponding hydrostatic pressures are then retrieved in an iterative upward fashion from
30 30 km at 1.5 km spacing. Finally the retrieved $T(p)$ profile is merged into the NCEP profile
31 from 34 km (pure NCEP) to 43 km (pure HALOE retrieval). Pressures are calculated

1 assuming hydrostatic balance. This entire process is repeated again after retrieval of water
2 vapor, and finally after a retrieval of aerosols, to account for all significant interfering
3 absorption in the 2.8 μ m CO₂ channel.

4 **2.3 ACE-FTS**

5 ACE-FTS was launched in August 2003 on board the SCISAT-1 satellite. SCISAT-1 is
6 operating in a circular, low-Earth orbit, with a 74° inclination and an altitude of 650 km
7 (Bernath et al., 2005). ACE-FTS measures ozone at IR wavelengths (9.6 μ m).

8 Figure 1c shows the ACE-FTS measurement locations during 2005. The latitude coverage is
9 approximately 85°S–85°N. The instruments measure up to 15 SR and 15 SS profiles each day.
10 Approximately six times per year, the tracks of the SR and SS measurements cross over.
11 Unlike SAGE II and HALOE, however, the sampling pattern changes little from year to year.
12 Thus, data for 10°S–10°N are obtained only in February, April, August, and October of each
13 year (see Figure 1c).

14 We analyzed the most recent data, version 3.0 (Dupuy et al., 2009; Waymark et al., 2013),
15 obtained between 2004 and 2011. Data were provided at geometric altitudes from 0 to 140 km,
16 with a spacing of 1 km. Some of the data obtained during this period had measurement
17 problems and were not used based on the recommendations from the ACE-FTS Data Issues
18 List (https://databace.scisat.ca/validation/data_issues.php).

19 Altitudes in ACE-FTS measurements are defined as follows (see Boone et al., 2005 for
20 details). At low altitudes (below ~42 km), pointing information from the satellite is relatively
21 poor and the pointing is quite variable, with refraction effects plus clouds and aerosols
22 affecting the instrument's pointing. Therefore, geometry is derived through analysis of the
23 ACE-FTS spectra. CO₂ volume mixing ratio is fixed to its "known" profile, and then CO₂
24 lines are analyzed to determine pressure and temperature. Hydrostatic equilibrium is used to
25 express the altitude separations between measurements in terms of pressure and temperature
26 during the retrieval, so geometry is determined simultaneously. At high altitudes (above 60-65
27 km), geometry is relatively well known from first principles (i.e., given the knowledge of the
28 location of the satellite and the look direction to the sun at a given time, one can calculate the
29 pointing information). In the middle (42-60 km), CO₂ VMR is still "known" and geometry is
30 known. This region allows us to determine the pressure at the "crossover" point (near 42 km)
31 to be used in the calculation of altitude at low altitudes (below ~43 km) via hydrostatic

1 equilibrium. A final altitude registration is performed using the Canadian Meteorological
2 Centre model output at the lowest altitudes (~15-25 km). The uncertainty on altitude
3 registration for the ACE-FTS is 150 m.

4 **2.4 SMILES**

5 SMILES was attached to the Japanese Experiment Module (JEM) on board the International
6 Space Station (ISS) through the cooperation of the Japan Aerospace Exploration Agency
7 (JAXA) and the National Institute of Information and Communications Technology (NICT).
8 The ISS is in a circular orbit at a typical altitude between 350 and 400 km, with an inclination
9 of 51.6°. Its latitude coverage is 38°S–65°N. SMILES measured the Earth's limb and made
10 global observations of the minor constituents in the middle atmosphere in the 600 GHz range
11 between 12 October 2009 and 21 April 2010 (Kikuchi et al., 2010). Unlike the solar
12 occultation measurements (SAGE II, HALOE, and ACE-FTS), limb emission measurements
13 are made continuously following the orbit track, not only at SR and SS, but throughout the
14 day and night. As a result, two datasets for ascending and descending nodes are obtained
15 every day, in each latitude band. In addition, the ISS is not in a Sun-synchronous orbit, and its
16 orbital plane rotates every 60 days; consequently, a full diurnal cycle in the tropics is covered
17 in 30 days by the ascending/descending nodes.

18 For SMILES, we defined the SS and SR profiles as those characterized by solar zenith angles
19 between 80° and 100°. Note, again, that SMILES measurements cover the full diurnal cycle,
20 as well as during SS and SR. Thus, the SSD related to diurnal variations in ozone level can be
21 calculated. With regard to the quality of ozone data from SMILES, Imai et al. (2013a)
22 compared the ozone concentration profiles from the SMILES version 2.1 dataset with those
23 from five satellite measurements and two CTMs (including SD-WACCM), and found that in
24 the stratosphere the agreement was generally better than 10%. Imai et al. (2013b) compared
25 the ozone concentrations profiles from the SMILES version 2.3 dataset with those from
26 worldwide ozonesonde stations and found that the agreement was between 6% and 15% for
27 20-26 km at low latitudes; part of this difference was attributed to issues related to the
28 ozonesonde measurement system.

29 In this study, version 2.4 data were analyzed (JEM/SMILES L2 Products Guide for version
30 2.4: http://smiles.tksc.jaxa.jp/l2data/pdf/L2dataGuide_130703.pdf). Data were provided at
31 geometric altitudes between 8 km and 118 km, with a vertical spacing of 2 km (below 58 km)

1 or 3 km (above 58 km). The number of retrieved profiles in version 2.4 was significantly
2 larger than that in version 2.0, by updating the screening conditions. We did not find any
3 significant differences in diurnal variation between versions 2.4 and 2.0 (which was used by
4 S13). For stratospheric diurnal variations in the SMILES data, Parrish et al. (2013) found
5 good agreement with the results from ground-based microwave measurements at Mauna Loa
6 (19.5°N, 204.5°E), as well as those from the Microwave Limb Sounder onboard the UARS
7 and Aura satellites.

8 SMILES does not measure geometric altitude, so that temperature (from SMILES below ~40
9 km and from SD-WACCM (for ver.2.4) above ~40 km) and pressure (from SMILES) are
10 used to calculate the "relative" altitudes from some pressure level, with the hydrostatic
11 equilibrium assumption. For deriving the "absolute" altitude, pressure at 30 km from SD-
12 WACCM output is used (for ver2.4) (C. Mitsuda, personal communication). The uncertainty
13 in altitude registration for SMILES is considered to be in the same order as that for other
14 datasets. Note that there is no systematic difference in the altitude registration between SR
15 and SS.

16 **2.5 SD-WACCM**

17 The NCAR Whole Atmosphere Community Climate Model, version 4 (WACCM4), is a
18 comprehensive numerical model spanning the range of altitude from the Earth's surface to the
19 thermosphere (Garcia et al., 2007; Kinnison et al., 2007; Marsh et al., 2013). WACCM4 is
20 based on the framework of the NCAR Community Atmosphere Model, version 4 (CAM4),
21 and includes all of the physical parameterizations of CAM4 (Neale et al., 2013) and a finite
22 volume dynamical core (Lin, 2004) for the tracer advection. A version of WACCM4 has been
23 developed that allows the model to be run with specified (external) meteorological fields
24 (Kunz et al., 2011). Here specified dynamics (SD)-WACCM is a chemical transport model
25 (CTM) that ~~nudges~~ uses WACCM4 temperature, horizontal winds, and surface pressure
26 ~~nudged~~-towards 6-hourly time series from MERRA reanalysis- (Rienecker et al., 2011) below
27 50 km. The CTM data was constrained by meteorological conditions with an hourly timescale,
28 so that they could be directly compared with our observational data. Note that the
29 stratospheric ozone concentration and its diurnal variations in the SD-WACCM data have
30 been analyzed and that the results agreed well with those based on the SMILES data (Imai et
31 al., 2013a; S13).

1 The horizontal resolution used was 2.5° in longitude and 1.9° in latitude, and the model time
 2 step was 30 min. We prepared and analyzed a satellite coincidence data subset, which was
 3 sampled at the nearest time and grid point to each satellite measurement. The measurement
 4 longitude, latitude, and time were used pertaining to an altitude of 30 km. In other words, we
 5 did not consider any altitude dependence of the longitude, latitude, or time for a given profile.
 6 This may cause estimation errors in the mesosphere, where the ozone concentration changes
 7 rapidly at SR and SS (e.g., S13). Data were provided at 88 pressure levels and mapped onto
 8 geometric altitude grids corresponding to those of the satellite datasets. The geometric altitude
 9 (z) is calculated from geopotential height (Z) by the equation,

$$10 \quad z = \frac{rZ}{\frac{g}{g_0}r - Z}, \quad (2)$$

11 where g is the gravity at (z, ϕ) , $g_0 (= 9.80665 \text{ m s}^{-2})$ is the reference gravity, r is the radius of
 12 the Earth (cf. Mahoney, 2008, available from the web site

13 http://mtp.mjmahoney.net/www/notes/pt_accuracy/ptaccuracy.html)

14 As well as the satellite coincidence dataset (only at SR and SS), we analyzed three-hourly,
 15 3D-gridded data obtained between 2008 and 2010 (hereafter referred to as the ‘full-grid’ data)
 16 to extract the full diurnal cycle. We only used data for these three years because of constraints
 17 on data storage. As well as ozone mixing ratio, vertical wind in geometric altitude (w) and
 18 chemical generation or loss (S) in SD-WACCM data are also analyzed to assess the
 19 dynamical and photochemical contributions to the SSD (cf. Equation (1)). On pressure levels,
 20 w is calculated on pressure levels from geometric altitude (z) and vertical velocity (ω), by
 21 using the fomula,

$$22 \quad w = \frac{Dz}{Dt} = \frac{\partial z}{\partial t} + \mathbf{u} \cdot \nabla_z + \rho g \omega, \quad (3)$$

23 where \mathbf{u} is horizontal wind, ρ is density, and g is gravity acceleration; then, the calculated w is
 24 mapped onto geometric altitude grids.

25

26 **3 Analysis Methods**

27 When calculating the SSD, careful consideration should be given to the sampling issues.

28 Figure 2 shows the number of SR (red) and SS (blue) profiles in the latitude range of 10°S–

1 10°N obtained during the observation period. We see that the SR and SS profiles are not
2 distributed evenly; e.g., there are no SR (SS) profiles from November to January (May to
3 July) between 2001 and 2005 for SAGE II. This indicates that if the SSD is calculated by
4 simply averaging all SR and SS profiles for a certain period (e.g., Kyrölä et al., 2013), it could
5 be significantly contaminated by seasonal/interannual variations in ozone concentrations. In
6 fact, Kyrölä et al. (2013) reported that the SSD profile for 2001–2005 was considerably
7 different to those recorded in the other periods (1985-1990, 1991-1995, and 1996-2000); we
8 attribute this to contamination caused by uneven sampling during this period. To resolve this
9 issue, we calculated the SSD in SR–SS pairs which have both SR and SS profiles measured at
10 almost the same time (see the open stars in Figure 1). A pair is defined such that it has more
11 than one profiles for both SR and SS within 15 days (30 days) for SAGE II and HALOE
12 (ACE-FTS). However, note that there is still a difference of 10–15 days in the SR and SS
13 measurement times for each pair. We found that changes in ozone levels during these 10–15
14 days also contaminate the SSD. Therefore, this effect was further assessed and removed (see
15 below).

16 Approximately eight pairs for both SAGE II and HALOE, and four pairs for ACE–FTS were
17 defined for each year (see Figure 1). The differences in measurement days between SR and
18 SS profiles were less than about 10 days (15 days) for SAGEII and HALOE (ACE–FTS). The
19 total number of pairs for the entire period was 128 for SAGEII, 86 for HALOE, and 25 for
20 ACE–FTS. There were no SS–SR pairs for SAGE II data after 2001, although the
21 measurements continued until 2005. Also, for ACE-FTS, SS-SR pairs are defined only in
22 February, April, August and October. Between 10 and 50 profiles were obtained for SR and
23 SS in each pair (see Figure 2).

24 Figure 3 shows the time series of the ozone mixing ratio at an altitude of 40 km (10°S–10°N)
25 based on HALOE data for the period 1992–1993. The mean profile for each SR and SS for
26 the i^{th} SR–SS pair (SR^i and SS^i) was produced by averaging the SR (red open circles) and SS
27 (blue open circles) data, respectively. Subsequently, for each pair, the original SSD (SSD_{org}^i)
28 was calculated as the difference between the mean SS and SR profiles (i.e., $SSD_{\text{org}}^i = SS^i -$
29 SR^i). Figure 4 shows individual SSD_{org}^i values averaged at altitudes of 40–45 km based on
30 HALOE data, and sorted by time of year (black closed circles). We note again that, although
31 the differences in measurement days between the SR and SS profiles are less than 10–15 days,
32 seasonal variations still produced significant differences during this period and contaminate

1 the SSD. In fact, this effect is not negligible in the stratosphere, where semiannual variations
 2 in ozone concentration associated with the stratospheric semiannual oscillation (SAO) exist
 3 (e.g., Ray et al., 1994). Thus, we attempted to further remove the contamination caused by
 4 seasonal variations, as follows.

5 For both SAGE II and HALOE, we assessed the background ozone concentration changes
 6 (O_{3_BG}) at each altitude using linear multivariable regression:

$$7 \quad O_{3_BG} = b + at + q_1 QBO_{10}(t) + q_2 QBO_{30}(t) + \sum_{n=1}^2 (c_n \cos(n\omega t) + s_n \sin(n\omega t)), \quad (4)$$

8 where t is expressed in days, $QBO_{10}(t)$ and $QBO_{30}(t)$ are the quasi-biennial oscillation (QBO)
 9 indices defined by monthly zonal winds at 10 and 30 hPa, respectively, at Singapore
 10 (Naujokat, 1986), and $\omega = 2\pi/365.25$ (rad day⁻¹). The QBO indices are used after
 11 normalization by one standard deviation and application of a 12-month running mean (e.g.,
 12 Gebhardt et al., 2013). For the regression, least-squares fitting was applied to the time series
 13 of the average of the SR and SS in each pair (i.e., $(SR^i + SS^i)/2$; the time series of open stars
 14 in Figure 3). The resulting O_{3_BG} is also shown in Figure 3 (solid curve). We see that O_{3_BG}
 15 changes by approximately 0.1 ppmv over 10 days, which is comparable with the SSD (see
 16 below and Figure 4).

17 The SSD caused by seasonal variation for the i^{th} pair (SSD_{seas}^i) was then evaluated as:

$$18 \quad SSD_{seas}^i = O_{3_BG}(t_{SS}^i) - O_{3_BG}(t_{SR}^i), \quad (5)$$

19 where t_{SS}^i and t_{SR}^i are the day of i^{th} SS and SR, respectively. Figure 4 also shows SSD_{seas}^i
 20 (blue closed circles). SSD_{seas}^i exhibits semiannual variations that follow the ozone SAO, with
 21 an amplitude of up to 0.1 ppmv at this altitude. Finally, the corrected SSD (SSD_{cor}^i ; red open
 22 circles in Figure 4) was calculated as

$$23 \quad SSD_{cor}^i = SSD_{org}^i - SSD_{seas}^i. \quad (6)$$

24 We expect that this SSD was only caused by diurnal variations and/or instrumental/retrieval
 25 bias .

26 For ACE-FTS, only four pairs were obtained during the months of interest every year
 27 because of the repeating orbit pattern. This leads to incorrect assessment of the seasonal
 28 variations (particularly of the SAO) by the above fitting procedure (not shown). Thus, the
 29 SSD for ACE (SSD_{cor}^i) was calculated using SSD_{org}^i from ACE-FTS data and SSD_{seas}^i from

1 HALOE data. That is, SSD_{seas}^i is calculated for 2004-2011, using the fitting coefficients
2 estimated from HALOE data during 1990-2005.

3 Having calculated the SSD for each SR–SS pair, the SSD_{cor}^i was binned and averaged using
4 monthly bins. For example, if the day of a SR-SS pair was 13 April, the relevant SSD_{cor}^i was
5 assigned to the April bin. Figure 4 shows the monthly average values of SSD_{cor}^i , as well as
6 those of SSD_{org}^i and SSD_{seas}^i . If SSD_{org} was used for the analysis (see the black curve), it
7 shows a semiannual variation with maxima in February and July/August/September; however,
8 this is partially the result of contamination from SSD_{seas} , which shows a semiannual variation
9 (ca. 0.1 ppmv) associated with the stratospheric SAO (see the blue curve; Ray et al., 1994).
10 When this contamination is removed, as is done in the present study, SSD_{cor} instead shows an
11 annual variation with a maximum between December and February (see the red curve). This
12 seasonal variation is discussed in Section 4.2.

13 Finally, the annual mean SSD was calculated as the average of the monthly mean SSD_{cor} .
14 Note that correction for SSD_{seas} is important in the context of the annual mean SSD as well.
15 For SAGE II and HALOE, whose measurements cover the entire year, the annual mean of
16 SSD_{cor} is nearly the same as that of SSD_{org} , because the annual mean of SSD_{seas} should be
17 zero. This is, however, not the case for ACE–FTS, which made tropical measurements only in
18 particular months (i.e., February, April, August, and October). In this case, the annual mean
19 of SSD_{seas} is not zero, but reaches a maximum of approximately 0.1 ppmv; thus, the annual
20 mean of SSD_{org} is not equal to that of SSD_{cor} (not shown).

21 For SMILES, two kinds of SSDs are calculated with different procedures. The first kind of
22 SSD is based on SR-SS pairs. SR–SS pairs that had more than 10 profiles for both SR and SS
23 were analyzed, and four SR–SS pairs met this requirement (3 November 2009, 31 December
24 2009, 29 January 2010, and 29 March 2010). Each pair had more than 200 profiles for both
25 SR and SS. In all cases, SR and SS measurements were taken about 5 days apart. Unlike the
26 solar occultation measurements, SMILES observed the 10°S–10°N region almost
27 continuously (see Section 2.4). Consequently, the changes in background ozone
28 concentration; i.e., O_3_{BG} in Equation (4), were defined as the time series of ozone
29 concentration over the region 10°S–10°N to which a five-day running mean was applied.
30 Then, SSD_{seas} was assessed using Equation (3) and SSD_{cor} was obtained from Equation (6).
31 The average of the four SSD_{cor} s will be used in Section 4.1, while the individual SSD_{cor} s are
32 used in Section 4.2 in the context of a discussion of their seasonal dependence. Next, the

1 second kind of SSD is the SSD caused by diurnal variations. This quantity is the difference in
2 ozone levels between 1800 LT (for SS) and 0600 LT (for SR), as derived from hourly diurnal
3 ozone-concentration variations in the SMILES data averaged over the period of operation
4 (October 2009–April 2010). The method for extracting hourly diurnal variations from
5 SMILES data was described in S13. Note that the times of SR and SS are 1800 LT (± 0.3 hr)
6 and 0600 LT (± 0.3 hr), respectively, for the region 10°S – 10°N .

7 For the SD–WACCM output for satellite coincidences (HALOE, SAGE II, and ACE–FTS),
8 the same method was applied as that used for each satellite dataset. In contrast, for the full-
9 grid SD–WACCM output, diurnal variations as a function of LT were extracted for each
10 latitude and altitude grid point, for each month, as follows. First, three hourly diurnal
11 variations in Universal time (UT) are calculated at each longitude, latitude and altitude grid
12 point. Then, along each latitude band, data at the same local time are averaged to obtain
13 diurnal variations as a function of LT (e.g., 0000 LT data are the average of (0000 UT, 0°E),
14 (0300 UT, 315°E), (0600 UT, 270°E), (0900 UT, 225°E), (1200 UT, 180°E), (1500 UT,
15 135°E), (1800 UT, 90°E) and (2100 UT, 45°E)). Using this data, as for SMILES, the SSD
16 caused by diurnal variations, that is, difference between 1800 and 0600 LT, was calculated.
17 For SD–WACCM, as was done by S13, the contributions from vertical transport and
18 photochemistry are estimated, by integrating Equation (1). Diurnal variations of vertical wind
19 (w') and photochemical generation or loss (S') are both derived from the full-grid SD-
20 WACCM output.

21

22 **4 Results**

23 **4.1 Annual Mean**

24 Figure 5a shows the annual mean vertical profiles of the SSD in ozone mixing ratio in the
25 region between 10°S and 10°N , using data from the three solar occultation measurements and
26 from SD–WACCM output during each satellite coincidence. We see that HALOE (blue solid
27 curve) and ACE–FTS (green solid curve) agree well with each other for the entire
28 stratosphere; SD–WACCM results at times of satellite coincidence (blue and green dashed
29 curves) are also quantitatively consistent in the stratosphere (below ~ 55 km). In the lower
30 stratosphere, at an altitude of around 25 km, the SR profiles exhibit 0.05–0.1 ppmv more
31 ozone than the SS profiles. This difference gradually decreases with increasing altitude and

1 reaches zero at about 30 km. In the upper stratosphere, at 40–45 km, the SS profiles exhibit up
2 to 0.2 ppmv more ozone than the SR profiles. Figure 5b shows the ratio of the SSD to the
3 average ozone mixing ratio during the analysis period. The SSD is between –2% and –3% at
4 around 20 km, and gradually increases to 5% at an altitude of 45 km. The SSD near the
5 stratopause is quantitatively consistent with the HALOE result of *Brühl et al.* (1996),
6 although they only analyzed two latitude bands at around 18°N and 18°S.

7 SAGE II (red solid curve) shows a similar result to HALOE and ACE–FTS, at least
8 qualitatively, but the SSD in the upper stratosphere is approximately twice as large as those
9 resulting from the other datasets. The SAGE II results are essentially consistent with the
10 results of McLinden et al. (2009) and Kyrölä et al. (2013), although the latter may be partially
11 contaminated by seasonal/interannual ozone variations (see Section 3). Considering that the
12 SD–WACCM results at SAGE II measurement locations (red dashed curve) are consistent
13 with those at both HALOE and ACE–FTS measurement locations, we suggest that the
14 anomalous SAGE II values were not due to the differences in the measurement
15 locations/times compared with HALOE or ACE–FTS. Possible causes will be discussed in
16 Section 5.

17 There is a disagreement in SSD between satellite measurements and SD-WACCM above 55
18 km (Figure 5). This may be due to the difference in diurnal variations between the model and
19 observations, as shown out by S13 for the altitude region between 50 km and 60 km. S13 also
20 found that such a difference was attributed to the difference in the lowest altitude of the
21 dominance of mesospheric diurnal variations that shows a marked day-night contrast (i.e.,
22 ozone concentration maximizes (minimizes) during the nighttime (daytime)). Another
23 possible reason for the disagreement in SSD is that the strong ‘horizontal’ gradient of ozone
24 concentration associated with the rapid ozone changes at SS/SR in the mesosphere was not
25 considered in the retrieval of satellite measurements (Natarajan et al., 2005).

26 Figure 5 also shows the two SMILES results. One is the SSD deduced from the solar zenith
27 angle (black solid curve), while the other is the difference between 1800 and 0600 LT caused
28 by diurnal variations (black dot-dashed curve). We see that the HALOE and ACE–FTS results
29 are strongly supported by the SMILES results, although the SMILES SSD is about 2%
30 smaller than that based on HALOE and ACE–FTS data at an altitude of approximately 45 km.
31 This may be because SMILES observations have only four SR–SS pairs in total whereas the
32 HALOE and ACE-FTS have 86 and 24 pairs, respectively. SD–WACCM results at SMILES

1 locations also exhibit a smaller SSD compared with SD–WACCM results at HALOE and
2 ACE–FTS locations (not shown). It should be noted that there is an agreement of the two
3 results derived from the SMILES data. Also, Figure 6 compares the SSD from SD-WACCM
4 results at HALOE measurement locations (gray solid curve) and that caused by diurnal
5 variations from full-grid SD-WACCM (black solid curve), and again shows a good agreement.
6 These findings indicate that the SSD is predominantly caused by natural diurnal variations in
7 ozone concentrations (i.e., not by instrumental/retrieval bias).

8 Based on the finding that the SSD is consistent between satellite measurements (at least
9 HALOE and ACE-FTS) and SD-WACCM, SD-WACCM data are further examined. Figure 7
10 shows diurnal variations in ozone mixing ratio at 42 km, 32 km and 26 km, as derived from
11 full-grid SD-WACCM data (black solid curve). The contribution from vertical transport by
12 atmospheric tides (red solid curve) and that from photochemistry (blue solid curve) are also
13 shown (see Equation (1) and Section 3). As shown by S13, the sum of the two processes
14 (black dashed curve) explain almost all characteristics of diurnal variations (black solid curve).
15 At 26 km, ozone levels reach a maximum in the morning and a minimum in the afternoon in
16 the lower stratosphere mainly due to tidal vertical transport, resulting in a negative SSD. At
17 32 km, ozone levels show a significant diurnal variation during the daytime due to
18 photochemistry but they are almost zero at SR and SS, resulting in almost zero SSD.
19 Chapman mechanism and NO_x chemistry are related to the photochemical variations
20 (Pallister and Tuck, 1983; Schanz et al., 2014). At 42 km, ozone levels show a diurnal
21 variation caused by both vertical transport and photochemistry. But, as is the case at 32 km,
22 photochemical processes do not contribute to the SSD significantly. In contrast, the vertical
23 transport generates higher ozone levels in the late afternoon than in the morning; this causes a
24 positive SSD. The vertical transport exhibits only small variations at 32 km because of the
25 small vertical gradient in the background ozone concentration, i.e.,

26
$$\frac{\partial[\overline{O_3}]}{\partial z} \approx 0 \quad (7)$$

27 in Equation (1) (see figure 7d of S13).

28 Figure 8 shows the amplitude and phase of diurnal migrating tide in vertical wind averaged
29 between 10°S and 10°N, as derived from SD-WACCM data. The amplitude exponentially
30 increases with altitude. The phase basically shows the downward progression but it is almost
31 constant around 40 km possibly due to the presence of trapped modes excited by ozone

1 heating (e.g., Sakazaki et al., 2013b). Consequently, the phase of vertical wind is similar in
2 the whole stratosphere; thus, the sign of SSD (i.e., negative at 20-30 km and positive at 35-50
3 km) is determined by that of vertical gradient in the background ozone concentration.

4 Figure 6 also shows the contributions from vertical transport and photochemistry to the
5 annual-mean SSD profile. It is clearly demonstrated that the SSD in the tropical stratosphere
6 is mainly caused by vertical transport while the contribution from photochemistry is
7 negligible. Note that a further analysis of SD-WACCM indicated that the photochemical
8 variations cause a SSD of ~0.1 ppmv at high latitudes (>40°), where they are not zero at SR
9 and SS (not shown; cf. Schanz et al., 2014). The relationship between the SSD and vertical
10 tidal winds will be further demonstrated in the next section, where we will examine the
11 seasonal variations of the SSD.

12 **4.2 Seasonal Variations**

13 This section examines seasonal variations in the SSD. It should be emphasized here that by
14 calculating the seasonal variations in SSD using solar occultation measurements, we could,
15 ~~for the first time,~~ obtain quasi-observational evidence of seasonal variations in stratospheric
16 vertical tidal winds, which are difficult to observe directly. This section mainly use HALOE
17 data, because the SSD based on the HALOE measurements covers a wider range of months.
18 Figure 98 shows the month–altitude distribution of the SSD, from HALOE and SD–WACCM
19 at HALOE locations. In the upper stratosphere at altitudes of 40–50 km, both datasets show
20 that the SSD reaches a maximum during the Northern Hemisphere winter between December
21 and February (0.2–0.3 ppmv; see also Figure 4). In the lower stratosphere, at 20–30 km, the
22 SSD reaches a minimum twice, in March–April and again in August–September.

23 These seasonal variations can be confirmed on the basis of other datasets. Figure 109 shows
24 the seasonal variations in the SSD averaged between altitudes of 40 and 45 km and also
25 between 22 and 28 km, as derived from the three solar occultation measurements, as well as
26 the SMILES and SD–WACCM data at satellite measurement locations. In the upper
27 stratosphere (see Figure 109a), all data are consistent in the sense that the SSD reaches a
28 maximum between December and February. Note that the SSD based on SAGE II data is
29 larger by a constant amount (ca. 0.2 ppmv) than that based on the other datasets, for the entire
30 year. In the lower stratosphere (see Figure 109b), all data (except for those from ACE–FTS)
31 also agree reasonably well in that the SSD reaches a minimum between March and April,

1 while another minimum is discernable between August and November. The disagreement
2 seen for the ACE–FTS data may be caused by the smaller number of SR–SS pairs, or because
3 SSD_{seas} was estimated using HALOE data rather than ACE–FTS data (see Section 3).

4 Based on the finding that the seasonal dependence of SSD in the SD–WACCM data is
5 consistent with those in the satellite data, the full-grid SD–WACCM data are further analyzed
6 to interpret the seasonal variations of SSD from the perspective of those of diurnal variations
7 in ozone concentration. Figure 110a shows the month–altitude distribution of the difference in
8 ozone mixing ratio between 1800 LT (for SS) and 0600 LT (for SR); i.e., the SSD due to
9 diurnal variations, as derived from the full-grid SD–WACCM data (see also the black dashed
10 curve in Figure 109). The seasonal dependence shown in Figure 110a agrees well with that in
11 Figure 98b, both in the upper stratosphere (the positive-SSD region) and in the lower
12 stratosphere (the negative-SSD region). We conclude that the seasonal dependence of the
13 SSD is mainly caused by that in the diurnal variations in ozone level. Figure 110b shows the
14 seasonal variation of the SSD related to vertical tidal transport only (Equation 1). Good
15 agreement between Figure 110a and b again indicates that the SSD can be largely explained
16 by diurnal variations caused by vertical tidal transport. It is also suggested that the seasonal
17 dependence of the SSD is caused by that of the tidal vertical winds.

18 Although tides are mainly composed of diurnal and semidiurnal components, the former
19 cause the SSD, because the semidiurnal cycle does not cause any difference between two
20 measurements taken 12 hours apart (i.e., normal SR and SS at 0600 and 1800 LT). Figure 124
21 shows the tropical month–latitude distributions of the diurnal migrating tide in the vertical
22 winds at 42 and 26 km, derived from the SD–WACCM results. At an altitude of 42 km, the
23 amplitude is greatest during the Northern Hemisphere winter, while a small secondary
24 maximum is discernable in the period August–September between 20°S and 10°S. At 26 km,
25 we see similar double maxima, one in February–March and the other in August–September.
26 The seasonal variations in vertical wind are consistent with those in temperature (e.g., Wu et
27 al., 1998; Sakazaki et al., 2012). Sakazaki et al. (2013b) attributed the double maxima to the
28 seasonal dependence of the background zonal winds; the meridional advection of the zonal
29 wind momentum peaks twice a year, producing the tidal seasonal variation in the stratosphere.
30 We conclude that the seasonal variation in the vertical tidal wind causes the variation of the
31 vertical transport of ozone (see Figure 110b), and, consequently, this results in the seasonal
32 variation of the SSD (see Figure 110a). The secondary maximum in August–September at an

1 altitude of 42 km, as seen in the vertical wind, does not appear in the SSD, probably because
2 we only analyzed the SSD in the region 10°S–10°N.

3

4 **5 Discussion and Concluding Remarks**

5 We quantified the SSD (sunset-minus-sunrise difference) for the tropical stratosphere based
6 on three different measurements of solar occultation (SAGE II, HALOE, and ACE–FTS)
7 supplemented by data from SMILES measurements and the SD–WACCM model. To quantify
8 the SSD, we addressed the importance of removing the effects of sampling issues on the SSD,
9 particularly contamination by seasonal variations in ozone level. If contamination by seasonal
10 variations in ozone concentration is not removed in advance (i.e., if monthly composites are
11 calculated for SSD_{org}^i), the SSD shows seasonal variations that are contaminated by signals
12 associated with the SAO. These sampling issues should be taken into account when correcting
13 the SSD to create homogenized datasets based on solar occultation measurements.

14 All data, except for those from SAGE II, indicated that the SSD is up to +0.2 ppmv in the
15 upper stratosphere at altitudes of 40–45 km, and up to -0.1 ppmv in the lower stratosphere at
16 around 25 km. SMILES and SD–WACCM results suggested that the SSD is caused by natural
17 diurnal variations in ozone concentration, particularly variations related to vertical transport
18 by tidal winds. SAGE II data showed qualitatively similar results, including the seasonal
19 dependence, but the SSD in the upper stratosphere was twice as large as in the other datasets.

20 The SSD also shows seasonal variations: it reaches a maximum during the Northern
21 Hemisphere winter at an altitude of 42 km, and minima in March–April and September–
22 October near an altitude of 26 km. Analysis of SD–WACCM output showed that the seasonal
23 variation in the SSD follows that of the tidal vertical winds. We believe that we have obtained
24 the first quasi-observational evidence of the tidal vertical wind and its seasonal dependence in
25 the tropical stratosphere. Therefore, we suggest that the ozone SSD is not a bias, but a useful
26 proxy for the vertical tidal wind.

27 Nevertheless, there is an uncertainty about the magnitude of SSD; the SSD from SAGE II
28 data is twice as large as that from other four datasets. With the analysis of SD–WACCM
29 output, this difference is found not due to the difference in measurement locations or times
30 among the datasets. The retrieval procedure in SAGE II has been greatly updated in SAGE II

1 version 7 data (Damadeo et al., 2013). We have so far no clear answer to the difference, and
2 there may be several possibilities as discussed in the following.

3 A SSD could occur if the measurement “altitude” is mistakenly defined at SR and/or SS. But,
4 the observed uncertainty in SSD of ~4% (the difference in SSD between SAGE II and the
5 others at 42 km) corresponds to the uncertainty in altitude of ~400 m (at 42 km, the ozone
6 mixing ratio changes 1% per 100 m in vertical); this seems unrealistic, because an uncertainty
7 of defined altitude is considered 20 m for SAGE II, 100 m for HALOE, and 150 m for ACE-
8 FTS.

9 ~~Another related issue may be the reproducibility of atmospheric tides in models and~~
10 ~~reanalyses. We found that the amplitude of diurnal tide in SD-WACCM is up to ~50%~~
11 ~~smaller in the upper stratosphere than that in data from the Sounding of the Atmosphere using~~
12 ~~Broadband Emission Radiometry (SABER) measurements (version 2.0 data) (not shown).~~
13 ~~Considering that the SSD is largely attributed to the magnitude of atmospheric tides in~~
14 ~~vertical wind, it might be possible that the SSD in SD-WACCM data might be underestimated.~~
15 ~~The weaker tidal signal compared to SABER measurements is also the case for several~~
16 ~~reanalysis data, as was shown by Sakazaki et al. (2012). Because satellite measurements~~
17 ~~partly depend on reanalyses in their retrieval processes, the diurnal variations in retrieved~~
18 ~~ozone amount might be partly biased. For example, the SAGE II retrieval of ozone requires~~
19 ~~knowledge of the Rayleigh extinction which is related to atmospheric density at the tangent~~
20 ~~altitude. For version 7.0 data, the MERRA data are used to calculate the Rayleigh extinction.~~
21 ~~If the MERRA data does not include a realistic diurnal variability in density, the SAGE II~~
22 ~~ozone SSD will be biased. If, for example, MERRA densities were too large at sunrise and~~
23 ~~too small at sunset, then the SAGE II ozone would be too small at sunrise and too large at~~
24 ~~sunset and give rise to a SSD that is too large. Accurate measurements of temperature as well~~
25 ~~as ozone over a full diurnal cycle would be helpful to resolve this issue.~~

26 Another related issue may be the reproducibility of tides in SD-WACCM and reanalyses.
27 Satellite measurements use, more or less, (re)analysis data for the altitude registration and/or
28 the retrieval process. It is found that the amplitude of diurnal tide in SD-WACCM and
29 reanalyses is up to ~50% smaller in the upper stratosphere compared to than in data from the
30 Sounding of the Atmosphere using Broadband Emission Radiometry (SABER) measurements
31 (version 2.0 data) (not shown; see Sakazaki et al. 2012 for the comparison between SABER

1 and reanalyses). This could affect any of the satellite datasets, but a further study is needed for
2 a more quantitative discussion.

4 **Acknowledgements**

5 SAGE II data were provided by the NASA Atmospheric Data Center. HALOE data were
6 provided by GATS, Inc., through their Website (<http://haloe.gats-inc.com/home/index.php>).
7 ACE–FTS data were provided by the ACE Science Operations Centre. The Atmospheric
8 Chemistry Experiment (ACE), also known as SCISAT, is a Canadian-led mission mainly
9 supported by the Canadian Space Agency and the Natural Sciences and Engineering Research
10 Council of Canada. SMILES data were provided by the ISAS/JAXA. Monthly zonal wind
11 data from Singapore were obtained from the University of Berlin through its Website
12 (<http://www.geo.fu-berlin.de/en/met/ag/strat/produkte/qbo/index.html>). SABER version 2.0
13 data were provided by GATS, Inc., through their Website ([ftp://saber.gats-](ftp://saber.gats-inc.com/custom/Temp_O3/)
14 [inc.com/custom/Temp_O3/](ftp://saber.gats-inc.com/custom/Temp_O3/)). We thank Koji Imai for his help in working with the ACE–FTS
15 data. We are also grateful to Erkki Kyrölä and Chris Boone for their helpful suggestions and
16 comments. T. Sakazaki was supported in part by the Japanese Ministry of Education, Culture,
17 Sports, Science and Technology (MEXT), through a Grant-in-Aid for JSPS Fellows
18 (25483400). T. Sakazaki and M. Suzuki were also supported by the International Space
19 Science Institute, Bern, Switzerland (ISSI Team #246, Characterizing Diurnal Variations of
20 Ozone for Improving Ozone Trend Estimates, <http://www.issbern.ch/teams/ozonetrend/>). This
21 study was supported in part by the MEXT through a Grant-in-Aid (25281006), the ISS
22 Science Project Office of ISAS/JAXA, and the Human Spaceflight Mission Directorate of
23 JAXA. All figures were drawn with the GFD–Dennou library.

1 **References**

- 2 Beaver, G. M., L. Gordley and J. M. Russell III, Halogen Occultation Experiment (HALOE)
3 altitude registration of atmospheric profile measurements: lessons learned and
4 improvements made during the data validation phase, Proc. SPIE 2266, Optical
5 Spectroscopic Techniques and Instrumentation for Atmospheric and Space Research, 266,
6 doi:10.1117/12.187564, 1994.
- 7 Bernath, P. F., et al., Atmospheric Chemistry Experiment (ACE): Mission overview, Geophys.
8 Res. Lett., 32, L15S01, doi:10.1029/2005GL022386, 2005.
- 9 Boone, C., D., R. Nassar, K. A. Walker, Y. Rochon, S. D. McLeod, C. P. Rinsland, P. F.
10 Bernath (2005), Retrievals for the atmospheric chemistry experiment Fourier-transform
11 spectrometer, Appl. Opt. 44, 7218-7231.
- 12 Brühl, C., et al., Halogen Occultation Experiment ozone channel validation, J. Geophys. Res.,
13 101, 10,217-10,240, 1996.
- 14 Damadeo, R. P., J. M. Zawodny, L. W. Thomason, and N. Iyer, SAGE version 7.0 algorithm:
15 application to SAGE II, Atmos. Meas. Tech., 6, 3539-3561, 2013.
- 16 Dupuy, E. et al., Validation of ozone measurements from the Atmospheric Chemistry
17 Experiment (ACE), Atmos. Chem. Phys., 9, 287-343, 2009.
- 18 Garcia, R. R., D. Marsh, D. E. Kinnison, B. Boville, and F. Sassi, Simulations of secular
19 trends in the middle atmosphere, 1950-2003, J. Geophys. Res., 112, D09301,
20 doi:10.1029/2006JD007485, 2007.
- 21 Gebhardt C., A. Rozanov, R. Hommel, M. Weber, H. Bovensmann, J. P. Burrows, D.
22 Degenstein, L. Froidevaux, and A. M. Thompson, Stratospheric ozone trends and
23 variability as seen by SCIAMACHY during the last decade, Atmos. Chem. Phys., 14,
24 14831-14846, 2014.
- 25 Huang, F. T., R. D. McPeters, P. K. Bhartia, H. G. Mayr, S. M. Frith, J. M. Russell III, and M.
26 G. Mlynchak, Temperature diurnal variations (migrating tides) in the stratosphere and
27 lower mesosphere based on measurements from SABER on TIMED, J. Geophys. Res.,
28 115, D16121, doi:10.1029/2009JD013698, 2010.

1 Imai, K., et al., Validation of ozone data from the Superconducting Submillimeter-Wave
2 Limb-Emission Sounder (SMILES), *J. Geophys. Res. Atmos.*, 118, 5750-5769,
3 doi:10.1002/jgrd.50434., 2013a.

4 Imai, K., et al., Comparison of ozone profiles between Superconducting Submillimeter-Wave
5 Limb-Emission Sounder and worldwide ozonesonde measurements, *J. Geophys. Res.*
6 *Atmos.*, 118, 12,755-12,765, doi:10.1002/2013JD021094, 2013b.

7 Kalnay, E., M. Kanamitsu, R. Kistler, W. Collins, D. Deaven, L. Gandin, M. Iredell, S. Saha,
8 G. White, J. Woollen, Y. Zhu, M. Chelliah, W. Ebisuzaki, W. Higgins, J. Janowiak, K. C.
9 Mo, C. Ropelewski, J. Wang, A. Leetmaa, R. Reynolds, Roy Jenne, Dennis Joseph, The
10 NCEP/NCAR 40-Year Reanalysis Project, *Bulletin of the American Meteorological*
11 *Society*, **77** (3), 437–471, 1996.

12 Kikuchi, K., et al., Overview and early results of the Superconducting Submillimeter-Wave
13 Limb-Emission Sounder (SMILES), *J. Geophys. Res.*, 115, D23306,
14 doi:10.1029/2010JD014379, 2010.

15 Kinnison, D. E., G. P. Brasseur, S. Walters, R. R. Garcia, F. Sassi, B. A. Boville, D. Marsh, L.
16 Harvey, C. Randall, W. Randel, J. F. Lamarque, L. K. Emmons, P. Hess, J. Orlando, J.
17 Tyndall, and L. Pan, Sensitivity of chemical tracers to meteorological parameters in the
18 MOZART-3 chemical transport model, *J. Geophys. Res.*, 112, D20302,
19 doi:10.1029/2006JD007879, 2007.

20 Kunz, A., L. L. Pan, P. Konopka, D. E. Kinnison, and S. Tilmes, Chemical and dynamical
21 discontinuity at the extratropical tropopause based on START08 and WACCM analyses, *J.*
22 *Geophys. Res.*, 116, D24302, doi:10.1029/2011JD016686, 2011.

23 Kyrölä, E., M. Laine, V. Sofieva, J. Tamminen, S.-M. Päivärinta, S. Tukiainen, J. Zawodny,
24 and L. Thomason, Combined SAGEII-GOMOS ozone profile data set for 1984-2011 and
25 trend analysis of the vertical distribution of ozone, *Atmos. Chem. Phys.*, 13, 10645-10658,
26 2013.

27 Lin, S.-J., A “vertically-Lagrangian” finite-volume dynamical core for global atmospheric
28 models, *Mon. Wea. Rev.*, 132, 2293-2307, 2004.

29 Marsh, R. M., and J. M. Russell III: A tidal explanation for the sunrise/sunset anomaly in
30 HALOE low-latitude nitric oxide observations, *Geophys. Res. Lett.*, 27, 3197-3200, 2000.

- 1 Marsh, D. R., M.J. Mills, D.E. Kinnison, J.-F. Lamarque, N. Calvo, and L. M. Polvani,
2 Climate change from 1850 to 2005 simulated in CESM1(WACCM), 73727391, *J. Clim.*,
3 26(19), doi:10.1175/JCLI-D-12-00558.1, 2013.
- 4 McCormick, M.P.: SAGE II: An overview, *Adv. Space Res.*, 7, 3219-3226, 1987.
- 5 McCormick, M. P., Zawodny, J. M., Veiga, R. E., Larsen, J. C., and Wang, P. H.: An
6 overview of SAGE I and II ozone measurements, *Planetary Space Sci.*, 37, 1567-1586,
7 1989.
- 8 McHugh, M., Hervig, M., Magill, B., Thompson, R. E., Remsberg, E., Wrotny, J., and Russell,
9 J. Improved mesospheric temperature, water vapor and polar mesospheric cloud
10 extinctions from HALOE. *Geophys. Res. Lett.*, 30(8), 2003.
- 11 McHugh, M., Magill, B., Walker, K. A., Boone, C. D., Bernath, P. F., and Russell, J. M..
12 Comparison of atmospheric retrievals from ACE and HALOE. *Geophys. Res. Lett.*, 32(15),
13 2005.
- 14 McLinden, C. A., S. Tegtmeier, and V. Fioletov, Technical Note: A SAGE-corrected SBUV
15 zonal-mean ozone data set, *Atmos. Chem. Phys.*, 9, 7963–7972, 2009.
- 16 [Natarajan, M., L. E. Deaver, E. Thompson, and B. Magill \(2005\), Impact of twilight gradients](#)
17 [on the retrieval of mesospheric ozone from HALOE, *J. Geophys. Res.*, 110, D13305,](#)
18 [doi:10.1029/2004JD005719.](#)
- 19 Naujokat, Barbara, 1986: An Update of the Observed Quasi-Biennial Oscillation of the
20 Stratospheric Winds over the Tropics. *J. Atmos. Sci.*, 43, 1873–1877.
- 21 Neale, R. B., J. Richter, S. Park, P. H. Lauritzen, S. J. Vavrus, P. J. Rasch, and M. Zhang, The
22 Mean Climate of the Community Atmosphere Model (CAM4) in Forced SST and Fully
23 Coupled Experiments, *J. Clim.*, 26(14), 5150-5168, doi:10.1175/JCLI-D-12-00236.1, 2013.
- 24 Newchurch, M. J., E.-S. Yang, D. M. Cunnold, G. C. Reinsel, J. M. Zawodny, and J. M.
25 Russell III, Evidence for slowdown in stratospheric ozone loss: First stage of ozone
26 recovery, *J. Geophys. Res.*, 108(D16), 4507, doi:10.1029/2003JD003471, 2003.
- 27 Pallister, R. C., and A. F. Tuck, The diurnal variation of ozone in the upper stratosphere as a
28 test of photochemical theory, *Q. J. R. Meteorol. Soc.*, 109, 271–284, 1983.

- 1 Parrish, A. et al., Diurnal variations of stratospheric ozone measured by ground-based
2 microwave remote sensing at the Mauna Loa NDACC site: measurement validation and
3 GEOSCCM model comparison, *Atmos. Chem. Phys. Discuss.*, 13, 31855-31890, 2013.
- 4 [Randall, C. E., et al., Validation of POAM III ozone: Comparisons with ozonesonde and](#)
5 [satellite data, *J. Geophys. Res.*, 108\(D12\), 4367, doi:10.1029/2002JD002944, 2003.](#)
- 6 Randel W., and F. Wu, Isolation of the ozone QBO in SAGEII data by singular-value
7 decomposition, *J. Atmos. Sci.*, 53, 2546-2559, 1996.
- 8 Ray, E. A., and J. R. Holton, The tropical semiannual oscillations in temperature and ozone as
9 observed by the MLS, *J. Atmos. Sci.*, 51, 3045-3052, 1994.
- 10 Rienecker, M. M., M. J. Suarez, R. Gelaro, R. Todling, J. Bacmeister, E. Liu, M. G.
11 Bosilovich, S. D. Schubert, L. Takacs, G-K Kim, S. Bloom, J. Chen, D. Collins, A. Conaty,
12 A. da Silva, W. Gu, J. Joiner, R. D. Koster, R. Lucchesi, A. Molod, T. Owens, S. Pawson,
13 P. Pegion, C. R. Redder, R. Reichle, F. R. Robertson, A. G. Ruddick, M. Sienkiewicz, J.
14 Woollen, MERRA: NASA's Modern-Era Retrospective Analysis for Research and
15 Applications, *J. Clim.*, 24(14), 3624-3648, doi:10.1175/JCLI-D-11-00015.1, 2011.
- 16 Remsberg, E., L. Deaver, J. Wells, G. Lingenfelter, P. Bhatt, L. Gordley, R. Thompson, M.
17 McHugh, J. M. Russell III, P. Keckhut, and F. Schmidlin, An assessment of the quality of
18 Halogen Occultation Experiment temperature profiles in the mesosphere based on
19 comparisons with Rayleigh backscatter lidar and inflatable falling sphere measurements. *J.*
20 *Geophys. Res. Atmos.*, 107(D20), 2002.
- 21 Russell, J. M. III, L. L. Gordley, J. H. Park, S. R. Drayson, W. D. Hesketh, R. J. Cicerone, A.
22 F. Tuck, J. E. Frederick, J. E. Harries, and P. J. Crutzen, The Halogen Occultation
23 Experiment, *J. Geophys. Res.*, 98, 10,777-10,798, 1993.
- 24 Sakazaki, T., M. Fujiwara, X. Zhang, M. E. Hagan, and J. M. Forbes, Diurnal tides from the
25 troposphere to the lower mesosphere as deduced with TIMED/SABER satellite data and
26 six global reanalysis data sets, *J. Geophys. Res.*, 117, D13108,
27 doi:10.1029/2011JD017117, 2012.
- 28 Sakazaki, T., M. Fujiwara, C. Mitsuda, K. Imai, N. Manago, Y. Naito, T. Nakamura, H.
29 Akiyoshi, D. Kinnison, T. Sano, M. Suzuki, and M. Shiotani, Diurnal ozone variations in
30 the stratosphere revealed in observations from the Superconducting Submillimeter-Wave

1 Limb-Emission Sounder (SMILES) on board the International Space Station (ISS), J.
2 Geophys. Res. Atmos., 118, 2991-3006, doi:10.1002/jgrd.50220, 2013a.

3 Sakazaki, T., M. Fujiwara, and X. Zhang, Interpretation of the vertical structure and seasonal
4 variation of the diurnal migrating tide from the troposphere to the lower mesosphere, J.
5 Atmos. and Solar Terr. Phys., 105-106, 66-80, 2013b.

6 Shiotani M., and F. Hasebe, Stratospheric ozone variations in the equatorial region as seen in
7 Stratospheric Aerosol and Gas Experiment data, J. Geophys. Res., 99, 14575-14584, 1994.

8 Schanz A., K. Hocke, and N. Kämpfer, Daily ozone cycle in the stratosphere: global, regional
9 and seasonal behavior modelled with the Whole Atmosphere Community Climate Model,
10 Atmos. Chem. Phys. Diss., 14, 5561-5609, 2014.

11 Wang, H. J., Cunnold D. M., and Bao X.: A critical analysis of Stratospheric Aerosol and Gas
12 Experiment ozone trends, J. Geophys. Res., 101, 12,495-12,514, 1996.

13 Waymark, C., K. Walker, C. Boone, and P. Bernath, ACE-FTS version 3.0 data set:
14 Validation and data processing update, Annals of Geophysics, 56, Fast Track-1,
15 doi:10.4401/ag-6339, 2013,

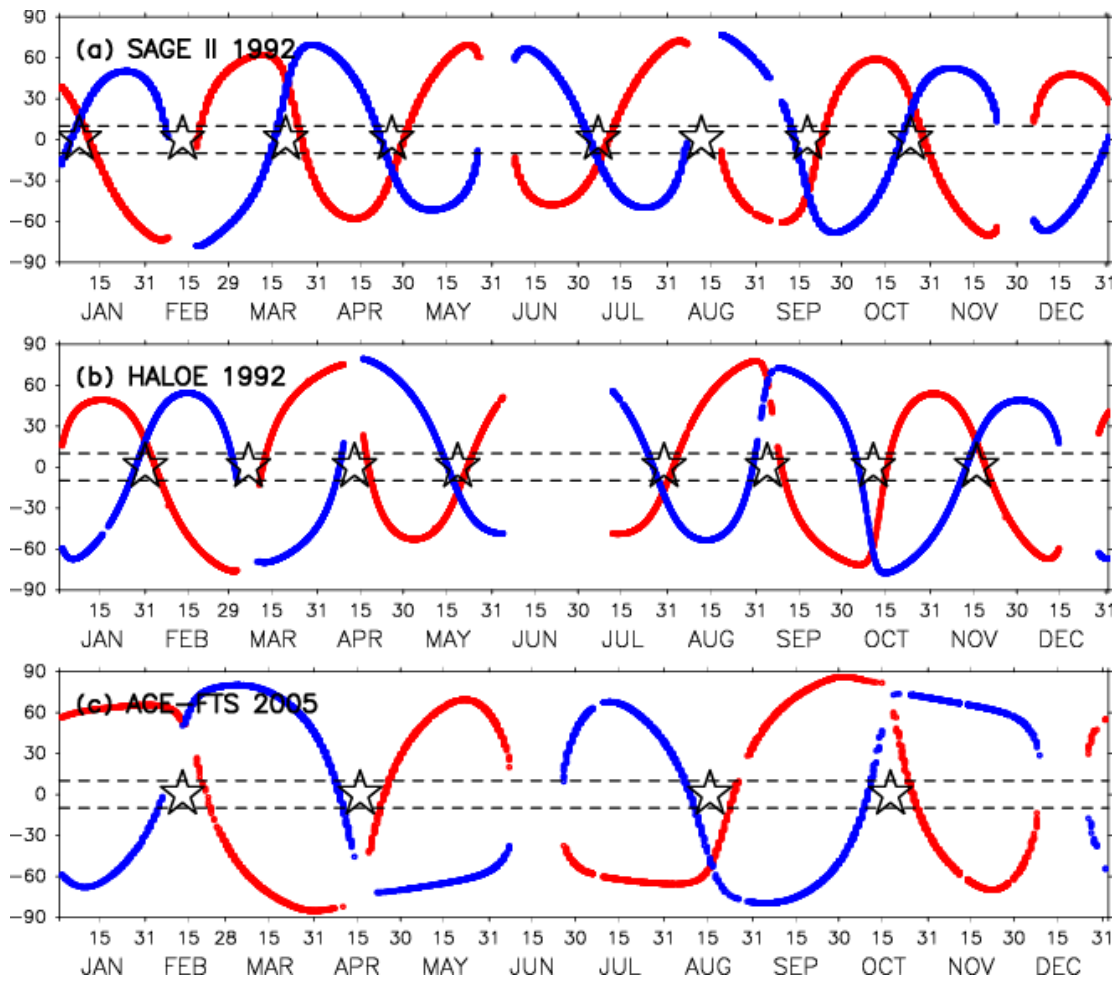
16 World Meteorological Organization (WMO), Scientific assessment of ozone depletion: 2010,
17 Report 52, Global Ozone Research and Monitoring Project, 2011.

18 Wu, D. L., C. McLandress, W. G. Read, J. W. Waters and L. Froidevaux, Equatorial diurnal
19 variations observed in UARS Microwave Limb Sounder temperature during 1991–1994
20 and simulated by the Canadian Middle Atmosphere Model, J. Geophys. Res., 103, 8909–
21 8917, 1998.

22 Zeng, Z., W. Randel, S. Sokolovskiy, C. Deser, Y.-H. Kuo, M. Hagan, J. Du, and W. Ward,
23 Detection of migrating diurnal tide in the tropical upper troposphere and lower
24 stratosphere using the Challenging Minisatellite Payload radio occultation data, J.
25 Geophys. Res., 113, D03102, doi:10.1029/2007JD008725, 2008.

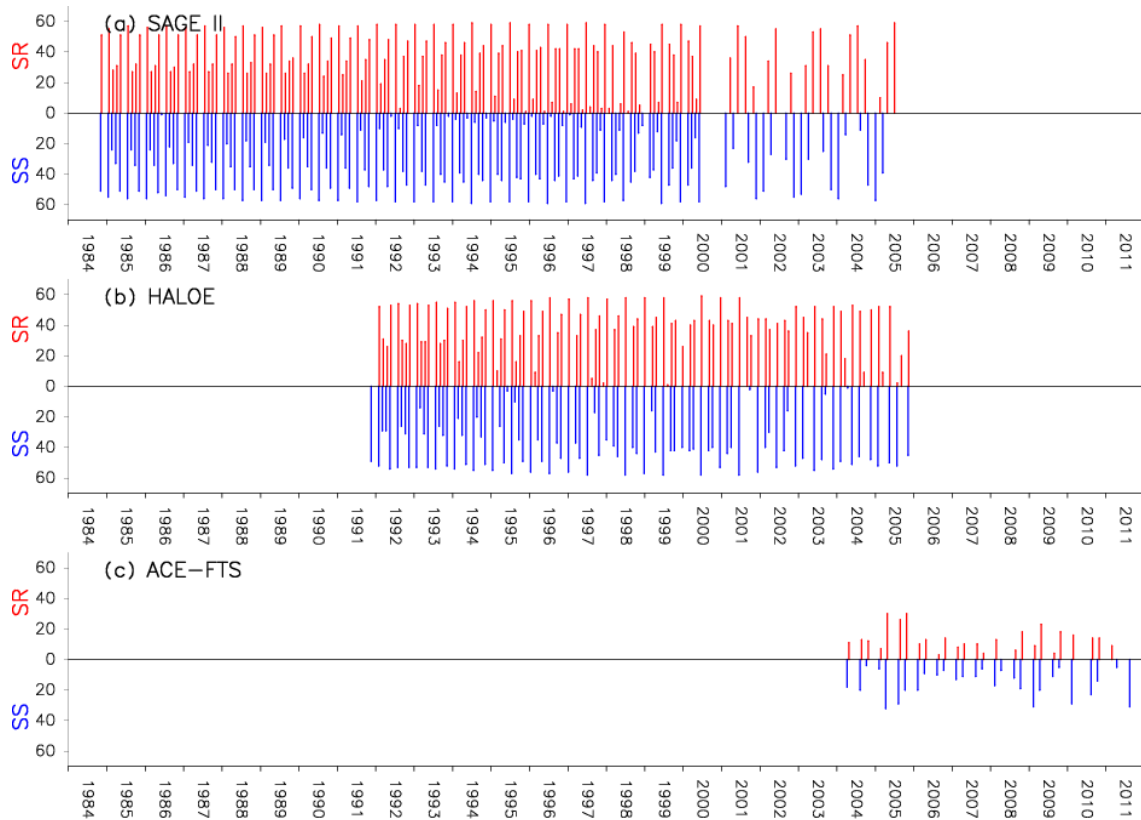
26

27



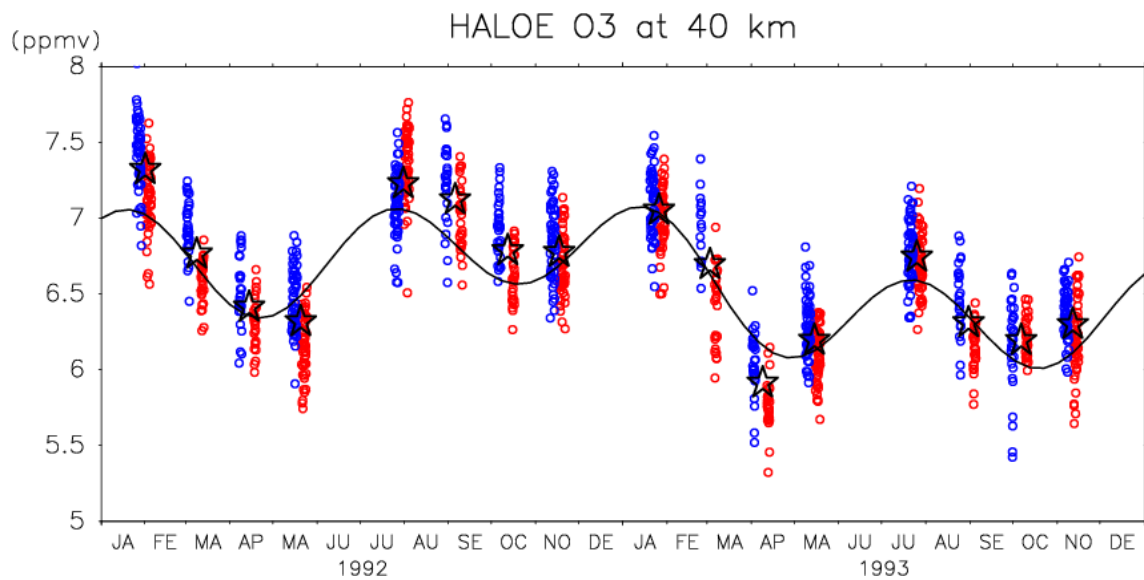
1
2
3
4
5
6

Figure 1. Measurement tracks of (a) SAGE II in 1992, (b) HALOE in 1992, and (c) ACE-FTS in 2005. Red and blue closed circles show SR and SS measurements, respectively. Open stars indicate SR-SS measurement pairs. Dashed lines denote 10°S/N.



1
2
3
4
5
6

Figure 2. Number of profiles obtained for observations at 10°S–10°N from (a) SAGE II, (b) HALOE, and (c) ACE-FTS. Red and blue bars show the number of SR and SS profiles, respectively.

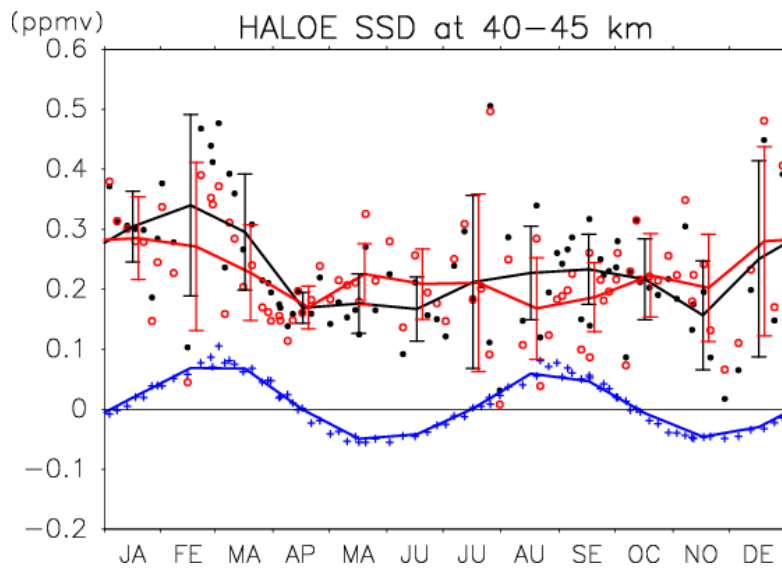


1

2 Figure 3. Time series of the ozone mixing ratio observed by HALOE during the period 1992–
 3 1993 at an altitude of 40 km (between 10°S and 10°N). Red and blue open circles show
 4 individual measurements at SR and SS, respectively. Open stars denote the average values of
 5 SR and SS, for each SR–SS pair. The solid curve shows the best-fit function for the average
 6 values (see Equation 4).

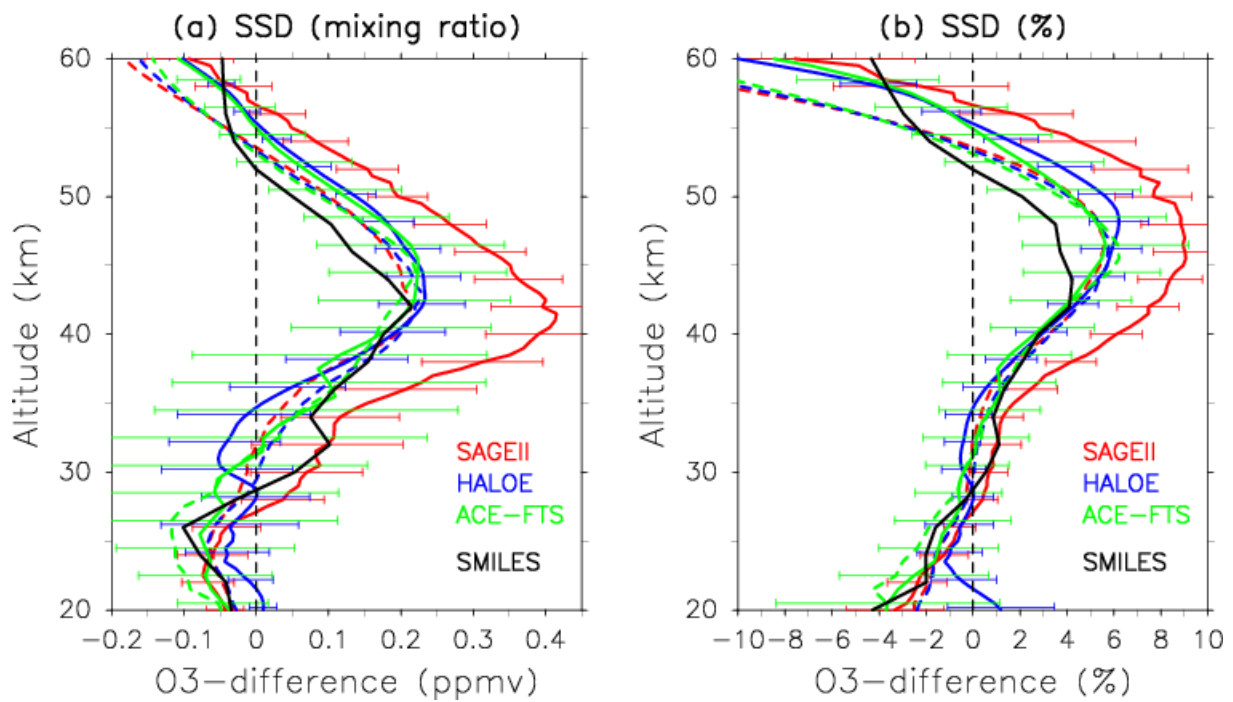
7

8



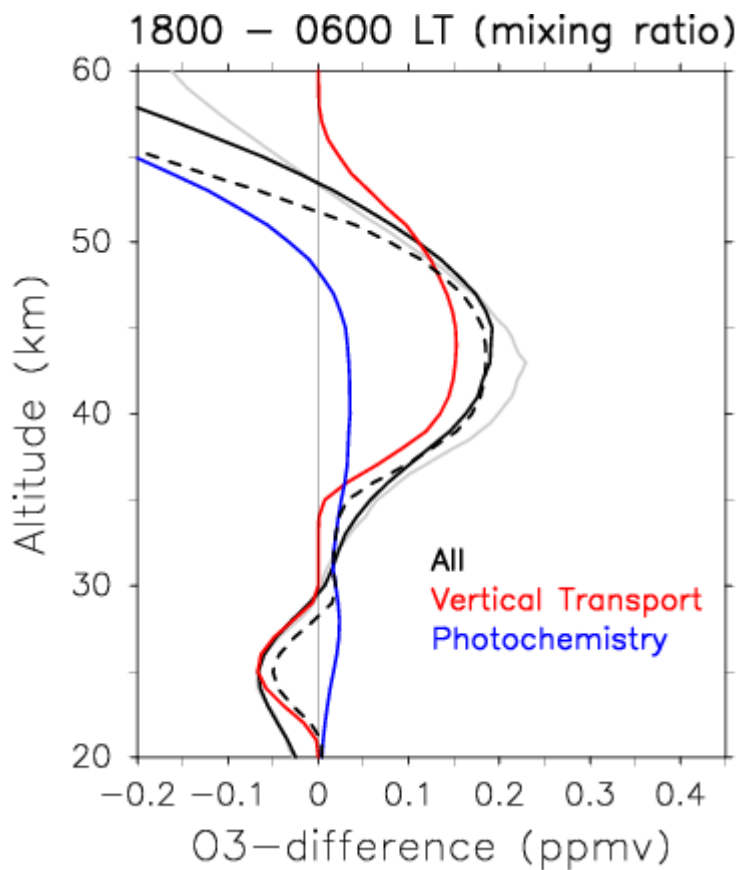
1
 2 Figure 4. SSD^{i}_{org} (black closed circles), SSD^{i}_{seas} (blue crosses), and
 3 SSD^{i}_{cor} (red open circles) averaged at an altitude of 40–45 km for individual
 4 SR–SS pairs sorted by time of year, derived from HALOE data during the period 1990–2005.
 5 Black, blue, and red curves denote monthly averaged SSD_{org} , SSD_{seas} , and SSD_{cor} ,
 6 respectively. Vertical bars show one standard deviation for the monthly SSD_{org} and SSD_{cor} .

7
 8



1
2 Figure 5. SSD_{cor} for $10^{\circ}S-10^{\circ}N$ in (a) ozone mixing ratio (ppmv), and (b) SSD ratio to the
3 daily mean (%), derived from SAGE II (red solid curves), HALOE (blue solid curves), and
4 ACE-FTS (green solid curves). Red, blue, and green dashed curves denote SD-WACCM
5 results at SAGE II, HALOE, and ACE-FTS coincidence, respectively. Black solid curves
6 show the SMILES result (SR and SS are defined by those profiles with a solar zenith angle
7 between 80° and 100°). Black dot-dashed curves show the difference between 1800 and 0600
8 LT, calculated using SMILES data and based on 1-hourly diurnal variations. Horizontal bars
9 for SAGE II, HALOE and ACE-FTS show 95% confidential levels in t -test. For the statistical
10 test, the error is defined as the standard deviation for the monthly SSD; this quantity has been
11 propagated to the error in annual-mean. Then, the t -test has been made with the degrees of
12 freedom being the total numbers of SS-SR pairs for each dataset.

13

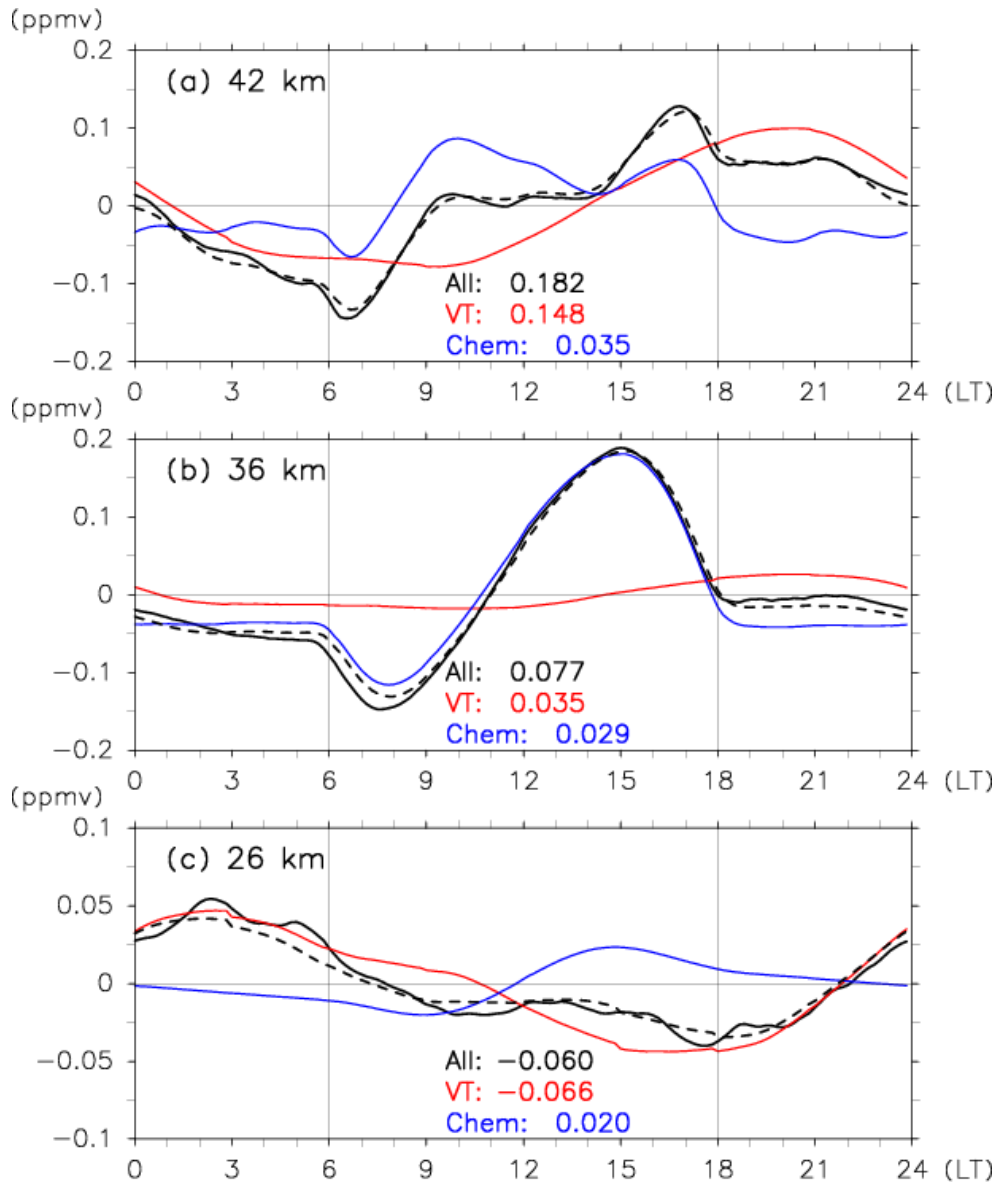


1

2 Figure 6. As Figure 5a, but for the difference between 1800 and 0600 LT, as deduced from
 3 diurnal variations in ozone concentration based on full-grid SD-WACCM between 2008 and
 4 2010. Solid curve is for the diurnal variations, red solid curve is for the contribution from the
 5 vertical transport, blue solid curve is for the contribution from photochemical processes, and
 6 the dashed solid curve is for the sum of tidal vertical transport and photochemical processes
 7 (see Equation (1) and Section 3 for details). Solid gray curve shows the SSD in SD-WACCM
 8 data at HALOE measurement locations (the same as blue dashed curve in Figure 5) for a
 9 reference.

10

11

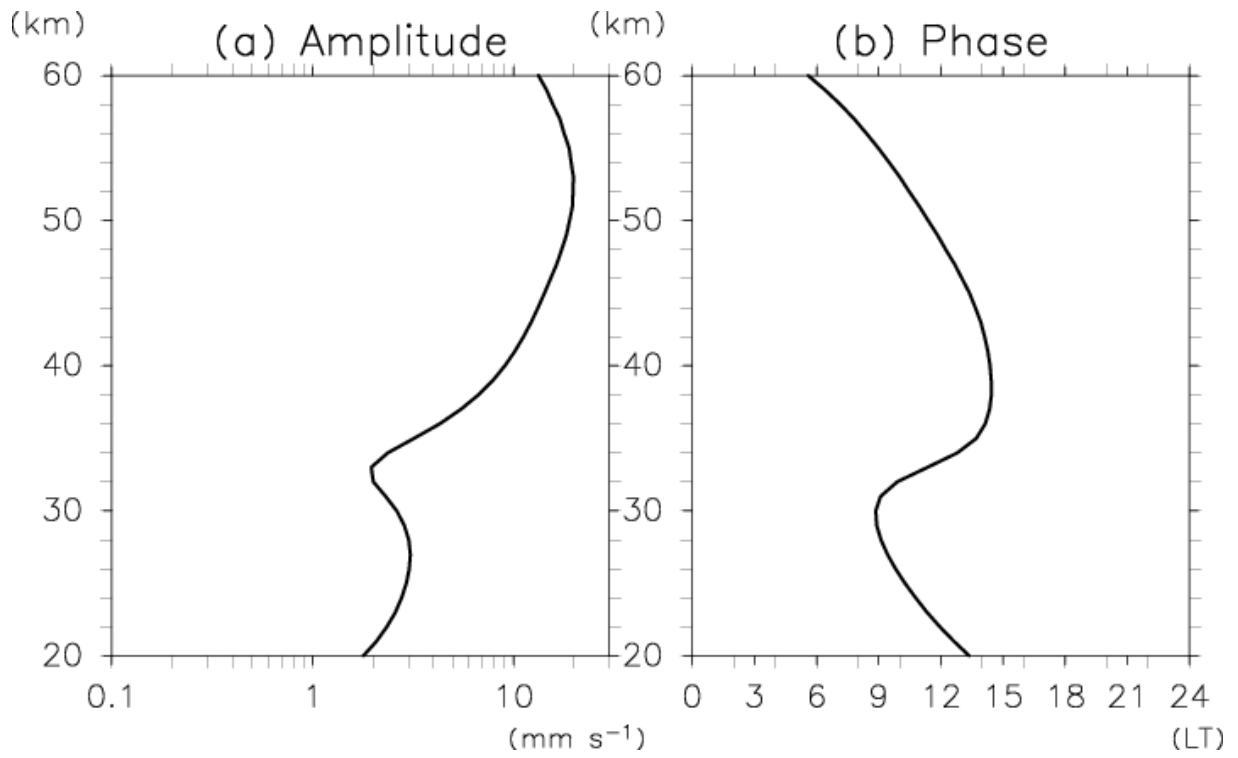


1
2 Figure 7. Diurnal variations in ozone mixing ratio averaged over 10°S-10°N at altitudes of (a)
3 42 km, (b) 36 km, and (c) 26 km. Black solid curves are SD-WACCM. Red solid curves show
4 the contribution from tidal vertical transport, and blue solid curves show the contribution from
5 photochemical processes (see Equation (1) and Section 3), while black dashed curves show
6 the sum of the two processes. SR and SS are denoted by thin black solid lines at 0600 LT and
7 1800 LT, respectively. The differences between 1800 and 0600 LT in ozone concentration
8 (ppmv) from diurnal variations (“All”), tidal vertical transport (“VT”), and photochemical
9 processes (“Chem”), are shown in each panel.

10

11

1

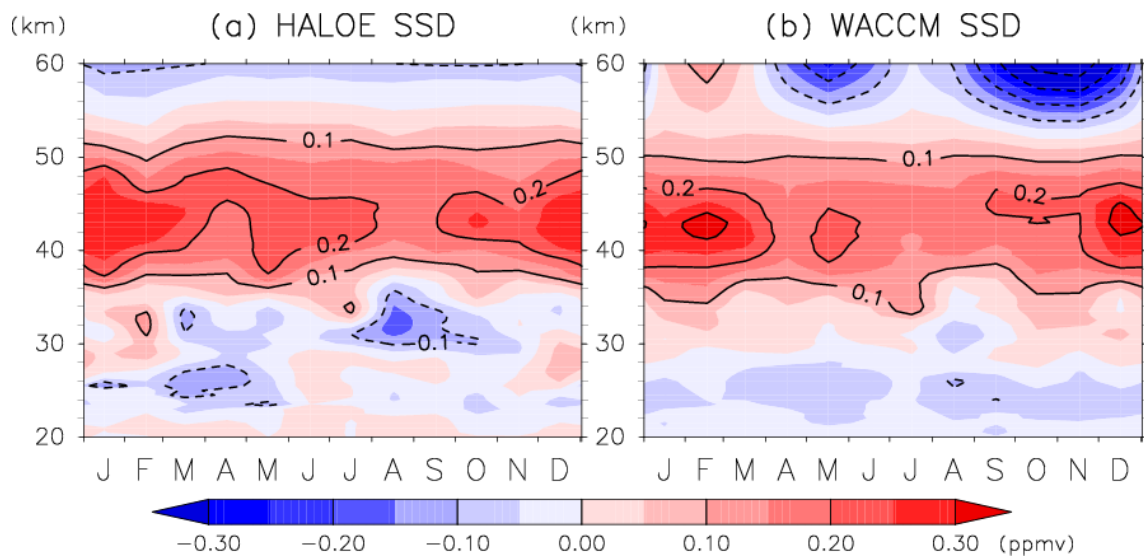


2

3 Figure 8: Vertical profiles of (a) amplitude and (b) phase for diurnal migrating tide in vertical
4 wind, averaged between 10°S and 10°N, as derived from SD-WACCM data during 2008-
5 2010.

6

7

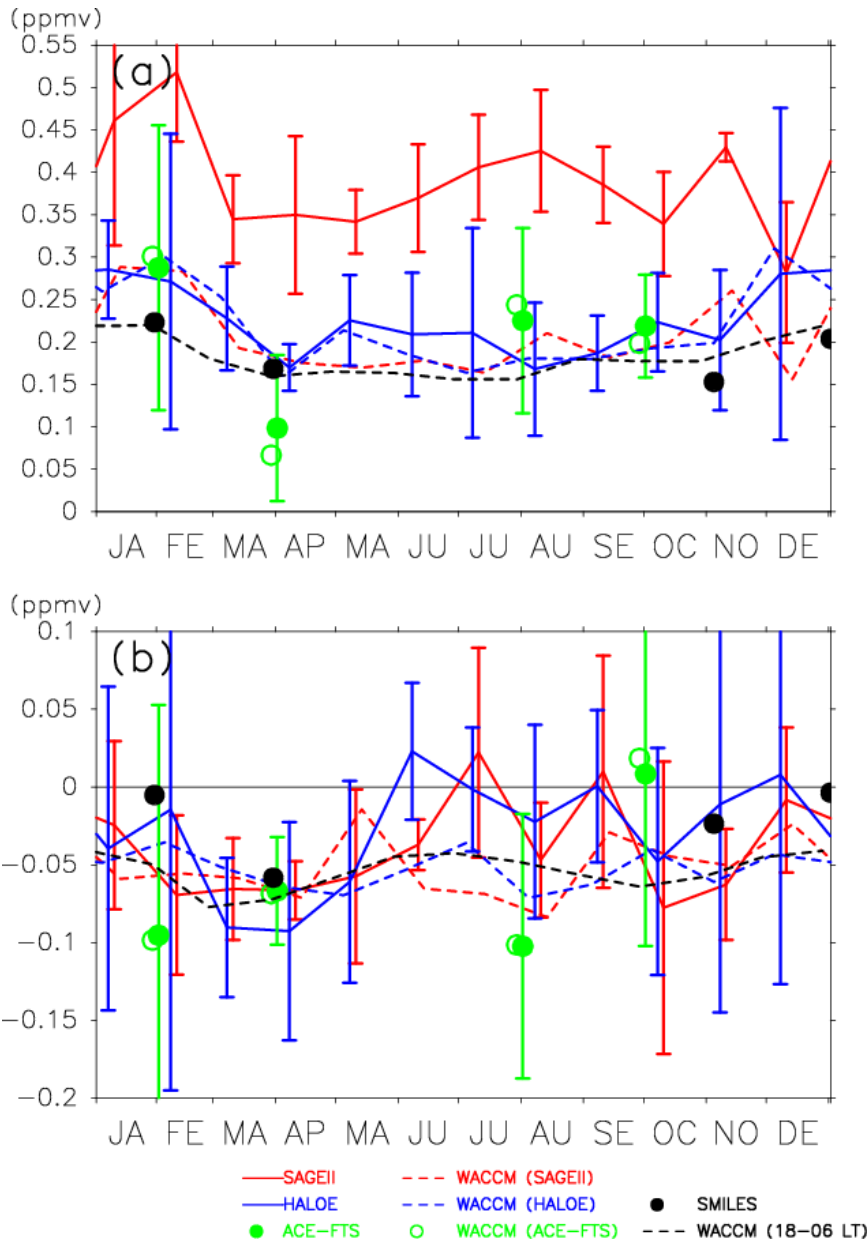


1

2 Figure 98. Month–altitude distributions of the SSD for the latitude range 10°S–10°N, derived
 3 from (a) HALOE and (b) SD–WACCM at HALOE measurement locations. Contour intervals
 4 are 0.1 ppmv.

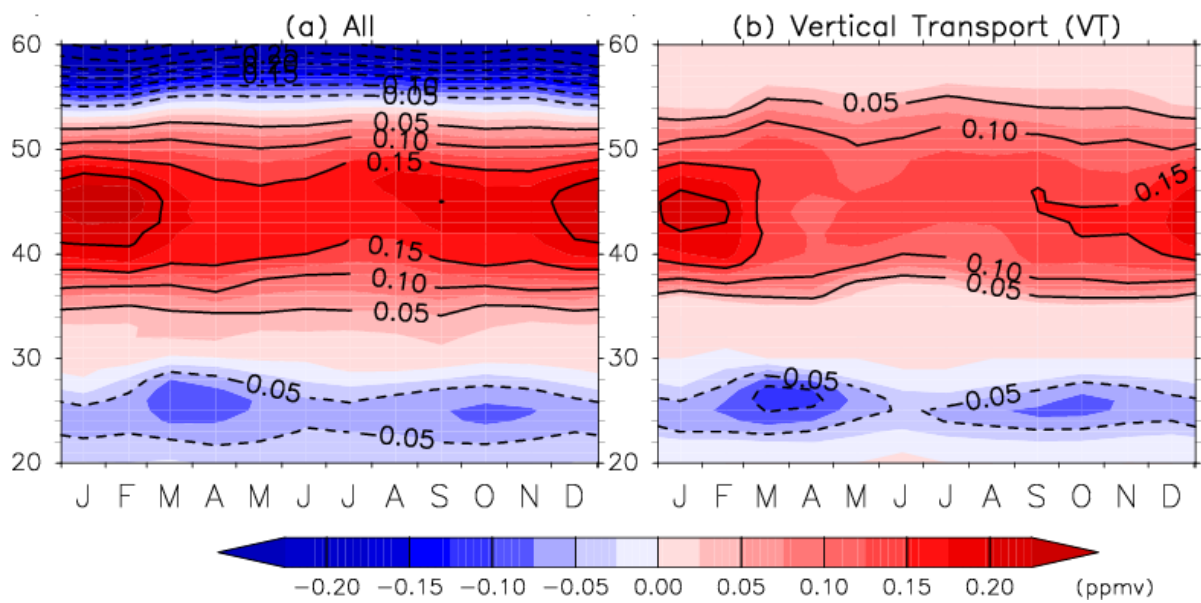
5

6



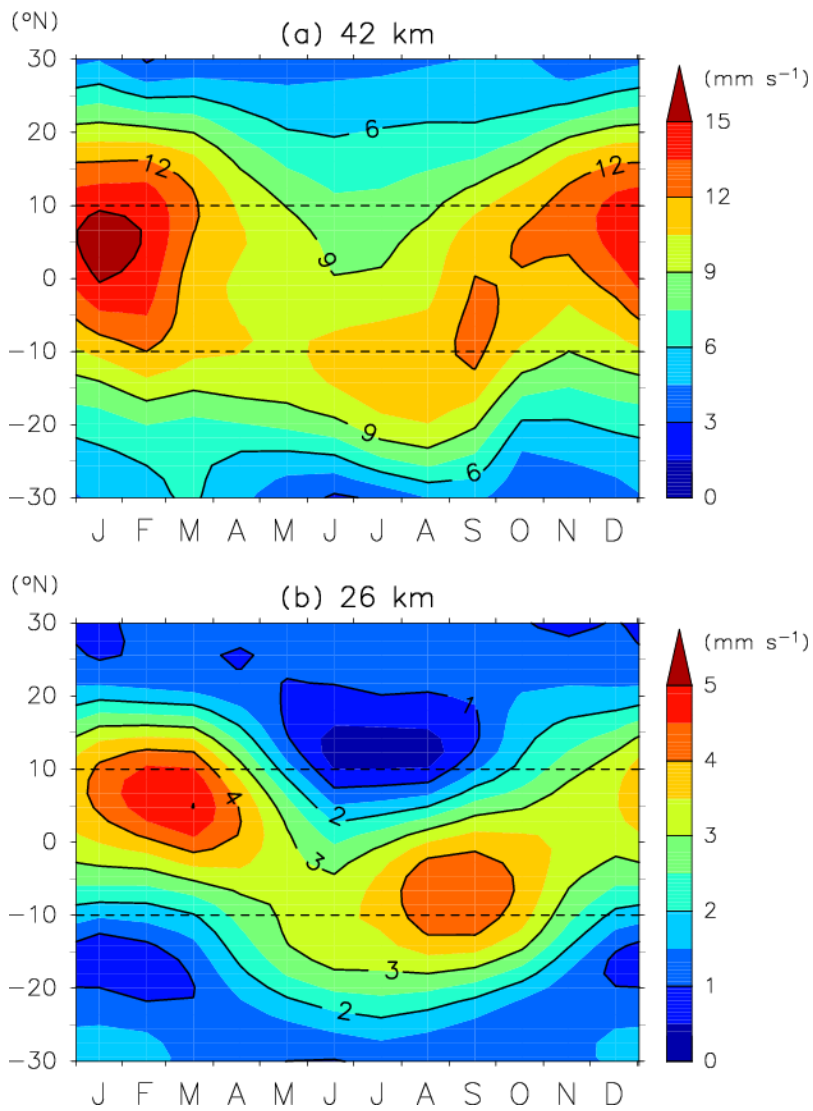
1
 2 Figure 109. Seasonal variation of O₃ SSD_{cor} at altitudes of (a) 40–45 km and (b) 22–28 km,
 3 obtained from (red solid curve) SAGE II, (red dashed curve) SD–WACCM at SAGE II
 4 locations, (blue solid curve) HALOE, (blue dashed curve) SD–WACCM at HALOE locations,
 5 (green closed circles) ACE–FTS, (green open circles) SD–WACCM at ACE–FTS locations,
 6 and (black closed circles) SMILES. The black dashed curve shows the difference in ozone
 7 between 1800 and 0600 LT, as deduced from diurnal variations in ozone concentration based
 8 on full-grid SD–WACCM between 2008 and 2010. Vertical bars for SAGE II, HALOE and
 9 ACE-FTS show 95% confidential levels with *t*-test.

10
 11



1
2
3
4
5
6

Figure 110. (a) As Figure 98, but for the difference in ozone mixing ratio between 1800 and 0600 LT, deduced from diurnal variations in ozone concentration based on full-grid SD-WACCM during the period 2008–2010. (b) As (a), but for the contribution from tidal vertical transport (see Equation 1).



1
 2 Figure 12.1. Month–latitude distributions of the amplitude of the diurnal migrating tide in
 3 vertical winds at altitudes of (a) 42 km and (b) 26 km, derived from SD–WACCM data for the
 4 period 2008–2010.

5